SPACE SCIENCES LABORATORY

FINAL REPORT

NASA Grant NGR 05-003-445

UCB Current Detector Experiment on Swedish Auroral Payloads

Principal Investigator

Professor Forrest Mozer

Period of Performance

January 1, 1972 to September 30, 1973

April 30, 1974

Space Sciences Laboratory Series 15 Issue 22

UNIVERSITY OF CALIFORNIA, BERKELEY

Space Sciences Laboratory
University of California
Berkeley, California 94720

FINÁL REPORT

NASA Grant NGR 05-003-445

UCB Current Detector Experiment on

Swedish Auroral Payloads

Principal Investigator

Professor Forrest Mozer

Period of Performance

January 1, 1972 to September 30, 1973

Space Sciences Laboratory Series 15 Issue 22

April 30, 1974

Table of Contents

Bibliography

Work Supported Wholly or in Part by
NASA Grant NGR 05-003-445

Bering, E.A., Properties of the wake of small Langmuir probes on sounding rockets, (in press), J. Atmos. Terr. Phys., 1974.

Bering, E.A., Auroral zone electric current measurements on sounding rockets, Ph.D. thesis, University of California, Berkeley, 1974.

Bering, E.A., M.C. Kelley and F.S. Mozer, Measurement of a parallel flux of thermal ions near an arc boundary, (abstract), Trans. Am. Geophys. Union, (in press), 1974.

Bering, E.A. and F.S. Mozer, Measurement of perpendicular current density in an aurora, (abstract), Trans. Am. Geophys. Union, 55, (4), 392, 1974.

Bering, E.A. and F.S. Mozer, Measurement of perpendicular current density in an aurora, (in preparation), 1974.

Bering, E.A., M.C. Kelley and F.S. Mozer, Measurement of a parallel flux of thermal ions and associated ion cyclotron turbulence,(in preparation), 1974.

Fahleson, U.V., E.A. Bering and several additional Swedish scientists (complete list uncertain), Properties and structure of auroral arcs inferred from multi-parameter measurements on sounding rockets, (in preparation), 1974.

I. Tasks Performed

The major project carried out under this grant was the measurement of electric current on two Nike Tomahawk sounding rockets launched by the Swedish Space Corporation from ESRANGE, Kiruna, Sweden on 7 February 1972 and 9 February 1973. The instruments used to make the measurement were split Langmuir probes. The work done may be divided into three phases: experiment design, construction and flight, and data analysis. The experiment design work included continuing efforts to understand the performance and behavior of the split Langmuir probe by analyzing data obtained from previous flights. The scientific results of this work, including previous flight results only partially supported by this grant, are summarized in section II of this report. The details of the scientific results of the Swedish flights alone are given in section III. The details of the instrument design which was developed for this project are given in section IV.

Most of the work done under this grant was carried out by a graduate student, Edgar Bering, who used the results for his Ph. D. thesis entitled "Auroral Zone Electric Current Measurements on Sounding Rockets" (University of California, Berkeley, 1974).

II. Summary of Scientific Results

An instrument, the split Langmuir probe, has been developed to make in situ measurements of ionospheric current density and plasma bulk flow. The split Langmuir probe consists of two conducting elements that are separated by a thin insulator that shield each other over a 2π solid angle, and that are simultaneously swept from negative to positive with respect to the plasma. By measuring the current to each plate and the difference current between plates, information can be obtained on the plasma's current density, bulk flow, electron temperature, and density.

Sources of error limiting complete measurement of all of these parameters include plate area differences, plate work function differences, input electronics differences, and probe wake effects. The instrument was successfully flown twice on sounding rockets into auroral events near local midnight on Swedish Nike Tomahawk 7/1 from ESRANGE, Kiruna, Sweden on 7 February 1972, and on Swedish Nike Tomahawk 7/2 from ESRANGE on 9 February 1973. In addition, data obtained from the split Langmuir probes flown on Javelin 8.56 VE from Fort Churchill, Manitoba, Canada on 3 April 1970 was analyzed. On the Javelin flight, the rocket passed repeatedly in and out of a bright folded arc structure. In the southern edge of the arc, the parallel detector measured a downward thermal ion current of 1.7×10^{-4} amperes/m^2 parallel to $\bar{B}$ in the earth-fixed frame. The latitudinal extent of this enhanced parallel flow was a few hundred meters. The upward return current was carried by precipitating electron within and to the north of the visual form. Current balance implies that parallel electron mobility was reduced in the region of the ion beam by an order of magnitude relative to expectation, apparently by anomalous resistivity. On the first Swedish flight, the electric field deduced from the ion flow velocity measurements and the electric field measured by the double probe experiment agree at altitudes above 140 kilometers to an accuracy well within the uncertainties of the two measurements. Below 140 kilometers, the two measurements diverge. This divergence gave a measurement of perpendicular current density, conductivity, and neutral winds. The height integrated current was 0.11 amperes/m flowing at an azimuth of 276°. This current was an order of magnitude too small to have been the main electrojet. The neutral winds were strong and to the south. On the second Swedish flight, the current measured on the upleg was 0.68 amperes/m flowing

at an azimuth of 55°. On the downleg, an equally strong southwestward current was indicated, implying the presence of oppositely directed electrojets. The neutral winds were strong and highly structured. The instrument is also ideal for studying the near wake of a small probe. Significant wake perturbations in plasma density and temperature were found due to the probe body itself, even though the probes were on the order of or smaller than the Debye length. The wake of small probes show apparent magnetic field aligned structure, even though the probes were much smaller than the ion gyroradius.

III. Results From Swedish Nike Tomahawks 7/1 and 7/2

A. Introduction

1. General Comments

The most recent two flights of the split Langmuir probe were on two identical Nike-Tomahawk payloads launched from ESRANGE, Kiruna, Sweden near local midnight on 7 February, 1972 and 9 February, 1973. These rockets were the seventh Nike Tomahawk payload configurations to be launched by the Swedish space research program and are customarily referred to as SNT 7/1 and 7/2.

A sketch of the payload is shown in Figure 1. Probe geometry and sweep characteristics are given in Tables I and II. Details of the probe and the instrument electronics are discussed in section IV. The other experiments on the payload relevant to auroral physics included a double probe electric field experiment provided by the Royal Institute of Technology, Stockholm; Langmuir probes, photometers, and a Faraday rotation experiment from the Uppsala Ionospheric Observatory; and an array of low energy electron and proton detectors from the Kiruna Geophysical Observatory.

2. SNT 7/1 Flight Conditions and Payload Performance

Payload 7/1 was launched into the recovery phase of a 400 γ auroral substorm. Figure 2 shows the ground magnetometer record from the period around the flight. A launcher malfunction sent the rocket on a course that was nearly due west. It is somewhat difficult to determine where the aurora was in relation to the rocket because darkroom mishaps destroyed the all-sky camera records from the sites that were clear, and there was broken cloud at the sites from which the various investigators were observing. Stoffregen (private communication) reported the auroral forms as corona. As viewed through broken cloud from the launch site, the aurora appeared to be brighter to the north of the trajectory, and to be brighter in the west than the east. It is hoped that analysis of the particle and photometer data will provide more information on the relative location of the rocket and the aurora than is now available.

There were several problems which limited, but did not seriously impair, experiment performance on the SNT 7/1 flight. As the result of an error in interpreting payload potential results from previous flights, the sweep stepped over plasma potential instead of sweeping through it. Therefore, it was impossible to measure electron temperature and plasma density or to attempt to make a direct measurement of current density. Another sweep potential related problem arose because the electron current being drawn from the plasma by the various experiments was rather large. As a result, the payload potential was very negative for about 40 seconds early in the flight. This effect interacted with the reference probe low pass filter described in section IV in such a way that the sweep was always positive from 80 to 120 seconds, and no ion flow data was obtained for this time period.

Payload mechanical performance also created a problem for the split probe experiment. The spin rate acheived was higher than nominal. The parallel probe was motor mounted, and was supposed to rotate 180° every 4 sweeps in order to measure any DC offsets. Because of weight constraints, the motor used generated only marginally enough torque to move the probe through a potential minimum at 90° rotation caused by the probe's flexing. At the higher spin rate, the motor torque proved insufficient, and the parallel probe stuck 90° out of alignment.

3. SNT 7/2 Flight Conditions and Payload Performance

Payload 7/2 was launched into a band of at least three parallel quiet arcs (Figure 3). These arcs occured during a relatively quiescent interval between two substorms on a moderately active night. The magnetogram from ESRANGE for that night appears in Figure 4. K_p was 4+ for the three hours before midnight and 4- for the three hours after midnight. Figure 4 indicates that there was about a 200γ magnetic disturbance at the time of launch. The rocket trajectory went almost north, and the projection for the trajectory down to 205 km along $\bar{B}$ traverses the southernmost half of the more intense visual forms appearing in Figure 3.

Malfunctions severely limited the quality and quantity of the data returned by the split Langmuir probe on SNT 7/2. The major problem was the appearance of a substantial 20kHz noise band on the PCM telemetry channel. The noise appeared after discrimination, and was therefore added to the signal before it entered the telemetry electronics. What appears to be the same noise band was detected by a swept frequency

analyzer measuring the AC electric field. From the character of the signal, it appears that it is being radiated by the rocket. It is believed that the cause of this noise was a time variable resistive break in the signal ground connection between the split Langmuir probe and telemetry. The effect of the noise on the split Langmuir probe data was to make the signal quite difficult to read after t = 120 seconds, and useless after t = 130 seconds except for a six second burst at t = 350 seconds.

Another significant problem was that the total plate to plate offset voltage was greater than $0.1\ kT_e/e$. This caused the DC offset in the difference current at plasma potential to be outside the dynamic range of the telemetry system, so that it was again impossible to make a direct measurement of current density.

B. Single Plate Langmuir Probe Measurements

No single plate data analyses were performed on the SNT 7 data. For the first flight, this was impossible since the sweep did not pass through plasma potential. On the second flight, the effect of sweeping slowly with respect to the rocket spin was to introduce a spin modulation on the single plate data that made analysis exremely difficult. The plasma density was also measured on this payload by several experiments provided by the Uppsala Ionospheric Observatory (UJO). Because of the difficulties with the split probe, the UJO data have been used for all of the analyses described in this chapter. The UJO results are plotted as a function of altitude in Figures 5 and 12. This data was provided with remarkable speed through the courtesy and efficiency of Bengt Holback.

C. Difference Current Measurements at Large Negative Potentials -- Ion Flow Measurements: Results From SNT 7/1

1. Methods of Data Analysis

The difference current data from SNT 7/1 were analyzed using the methods described in Bering (1974) with one addition and one exception. The addition to the analysis procedure resulted from the fact that the quasi-cylindrical geometry employed behaved very much like a cylinder in its focusing properties. Therefore, the focusing factor was modeled using the results of Bettinger and Walker (1965) with a single point normalization as described in Chapters III and V of Bering (1974). The exception arose when it became apparent that the wake correction described in section III.A.2.f of Bering (1974) increased the discrepancy between the split and double probe data rather than decreasing it. This correction is only used to illustrate the possible range of systematic errors.

2. Parallel Flow

The inability of the parallel probe motor to turn the parallel probe means that only the two components of ion flow velocity normal to the spin axis of the rocket have actually been measured. In order to transform these data into the earth-fixed geomagnetic reference frame it is necessary to determine the flow velocity parallel to the rocket. Since the rocket precession period was 22 seconds, it is possible to use the precession analysis method described by Bering. The method involves deducing the perpendicular components of the apparent electric field in earth-fixed geomagnetic coordinates for various assumptions of v_B, the component of plasma velocity parallel to $\bar{B}$. The correct choice of v_B is the one which minimizes the apparent precession periodicity in the deduced electric field.

The electric field components deduced from the SNT 7/1 ion flow data for various assumptions of v_B appear in Figure 6. Positive v_B is upward along $\bar{B}$. Detailed study of the results presented in Figure 6 indicates that a choice of v_B that is time varying and substantially different from zero is required to minimize apparent precession periodicity in the results. The results of this study appear in the bottom panel of Figure 7 labeled "best fit" and in the bottom panel of Figure 8. The values range from +1 km/sec before t = 150 seconds to -0.6 km/sec around t = 320 seconds, and are somewhat antisymmetric about apogee.

These apparent parallel flow velocities present a substantial problem in interpretation. The maximum apparent parallel ion velocity, 1 km/sec, is an order of magnitude greater than is seen by the Chatanika radar (Baron, private communication; Mozer and Cullers, private communication). The anti-symmetry about apogee is also very suspicious.

There are four possible interpretations of the v_B results. First, they could represent a real geophysical situation. This is extremely unlikely in view of the Chatanika results and the apogee anti-symmetry. Second, if the data before t = 160 seconds is dismissed as the result of outgassing and other post-deployment settling down effects (Haerendel et al., 1974), the data is not outside the realm of what has been seen before, and could represent a real geophysical situation. The magnitudes shown are still large enough for this interpretation to be regarded as substantially unlikely. Third, this result could be the result of a subtle malfunction internal to the instrument. The excellent agreement between the split and double probe data reported below argues strongly against this interpretation. Fourth, it could be caused by a rocket-plasma interaction of some sort which perturbs the component of ion velocity parallel to $\bar{B}$.

As can be seen in Figure 7, the best fit results for v_B are approximately consistent with the ion velocity parallel to $\bar{B}$ being zero in the rocket frame prior to t = 300 seconds. Similar results have been seen by another experimentor using a different technique on other flights (M. C. Kelley and J. -J. Berthelier, private communication). This other technique involves deducing the ion flow velocity from the phase of the wake observed with an ordinary probe at three positions around the precession cone of the rocket. Analyses of sounding rocket probe and particle data using this technique have given a similar result--namely, that the parallel ion velocity is zero in the rocket frame, or nearly so. Results from this technique do not always agree with double probe results from the same rockets, and must, therefore, be treated with extreme caution. Nonetheless, it does appear that the fourth interpretation of the v_B results--that they are an artifact of the rocket-plasma interaction--is the most likely one.

This phenomenon has not been previously reported in the literature. In view of its extreme interest to many sounding rocket investigators, it deserves more investigation. Several other properties can be deduced from the available split Langmuir probe data. First, it is not a universal phenomenon. The split Langmuir probe data gives no evidence of the effect on the Black Brant (Bering et al., 1973) or Javelin rockets (Bering, 1974). Second, it appears to be a DC phenomenon, and to be a slowly varying function of rocket velocity. It certainly does not prevent abrupt changes in v_B from being detected, and probably does not affect the validity of results based on detection of such changes in parallel difference current. Finally, it does not appear to be related to or to invalidate measurements of parallel electric fields, since the effect has been observed both on flights where

large $E_{\parallel}$ was observed and on flights where large $E_{\parallel}$ was not observed. Conversely, it has been absent in both circumstances. In conclusion, the SNT 7/1 parallel flow results appear to indicate the presence of a new and puzzling rocket-plasma interaction requiring further study before it can be fully understood.

3. Perpendicular Flow

The problem of interpreting the parallel results has implications as far as the perpendicular flow results are concerned. It is unclear which is the best procedure to follow in analyzing the data: use the best fit values for v_B, use $v_B = v_{rocket,B}$, or use $v_B = 0$. For purposes of comparison, all three possibilities are plotted in Figure 7 along with the results of applying the wake correction to the best fit results. The major conclusion that can be drawn from Figure 7 is that it does not make an enormous amount of difference which analysis procedure is chosen. Therefore, the results using the best fit values for v_B will be used for the rest of the analyses described below. In order to illustrate the range of possible systematic errors in subsequent analyses using the perpendicular data, the analyses were performed at selected times on all the results shown in Figure 7..

The electric field was also measured on the SNT 7 payloads by a double probe experiment provided by Ulf Fahleson of the Royal Institute of Technology, Stockholm, Sweden. Dr. Fahleson was kind enough to transmit the data from one pair of spheres via hardwire in the payload to the PCM encoder in the split Langmuir probe. In addition, he was kind enough to consent to analysis of this data at the University of California as part of this research, prior to his analyzing the data.

The double probe electric field data has been analyzed using the method of Kelley (1970) and compared with the results of the split Langmuir probe analysis (Figure 8). Above 140 km in altitude, the two sets of results are in excellent agreement, being well within the errors in the measurements. This agreement is substantially better than any reported in previous chapters, and represents further confirmation that the two experiments are measuring the ambient electric field. The difference between the two results which develops below 140 km on the downleg does not appear to be the result of errors in the measurement. Instead, it is due to the effect of ion-neutral collisions on ion mobility, and can be transformed into a measurement of perpendicular current density.

4. Current Density

The current density in an ionized medium can be deduced from the relationship

$$\bar{j} = ne\,(\bar{v}_i - \bar{v}_e) \qquad (1)$$

if the ion and electron velocities are known. In the ionosphere, electron mobility is not substantially affected by collisions above about 90 km. It is possible, therefore, to deduce the electron flow velocity above 90 km from the double probe electric field measurements using

$$\bar{v}_e = \bar{E} \times \bar{B} \,/\, B^2 \qquad (2)$$

The SNT 7/1 ion flow and electric field data have been analyzed using Equations 14 and 15 to yield a measurement of perpendicular current density. The results of these calculations are plotted as a function of altitude in Figure 9.

The data indicates that the rocket passed through a predominately westward electrojet, with a maximum current density of 5×10^{-6} amperes/meter^2 occuring at an altitude of 110 kilometers. The total height integrated current was 0.11 amperes/meter flowing at an azimuth of 276°. The error bars shown in the figure represent the statistical uncertainty in the measurement. In order to estimate the possible impact of systematic errors, the data has been analyzed at selected points using the other possible values for the parallel flow and wake correction shown in Figure 7. The scatter in the results of the various analyses is not significantly greater than the calculated error bars. Comparison of the size of the error bars with the magnitude of the measured current leads to the conclusion that the split Langmuir probe experiment on SNT 7/1 was accurate enough to make the current density measurement shown in Figure 9 valid and meaningful.

The current density measurements are in qualitative agreement with previous work. For example, Park and Cloutier (1971) reported a magnetometer measurement of the electrojet in an aurora in which they deduce a current density of 1.5×10^{-5} amperes/meter^2 in a westward electrojet. Also, they agree with theoretical electrojet models such as the one developed by Boström (1964).

Since substorms are highly variable phenomena and can vary in intensity over several orders of magnitude, it is far more useful to compare these results with the ground magnetometer data from the same substorm. At t = 300 seconds, the magnetic disturbance at launch was $\Delta x = -204$, $\Delta y = 116$, $\Delta z = -60$. The measured current is too small by an order of magnitude, and is oriented 3.5° too far to the north to have produced the measured ground disturbance. It appears, therefore, that

the rocket did not pass through the main electrojet. From the sign of z, and the observed location of the aurora, it appears that the rocket passed to the south of the region of maximum electrojet intensity.

5. Conductivity

Conductivity is formally defined by the relationship between electric field and current density. If both of these quantities are known, it is a simple task in algebra to calculate the conductivity. In a magneto-plasma, the problem is slightly complicated by the fact that conductivity is not a simple scalar, but rather a tensor. Perpendicular to $\bar{B}$, there are two components of current density--parallel and perpendicular to the electric field--and two different corresponding elements in the conductivity tensor. These are known as the Pedersen and Hall conductivities respectively. These quantities have been calculated for the SNT 7/1 flight using the data shown in Figures 8 and 9. The results have been plotted as a function of altitude in Figure 10.

The data indicate a maximum Hall conductivity of 1.1×10^{-4} mho/meter at 110 km and a maximum Pedersen conductivity of 1.4×10^{-4} mho/meter at 117 km. The height integrated Hall conductivity was 3.0 mho and the height integrated Pedersen conductivity was 3.1 mho. The same comments about the size and relative importance of statistical and systematic errors that were made above in regard to current density apply here as well. It should be noted that the error bars are somewhat larger in percentage terms than in the previous section, a result to be expected since the measurement is an additional step away from the raw data.

A model conductivity profile has also been plotted in each

panel of Figure 10 for purposes of comparison. Since the most recent related experiment to be reported is the one performed by Brekke et al. (1973), the model conductivity calculations were done wherever possible by the same methods in order to insure maximum comparibility of results. Specifically, the same approximation for the ion cyclotron frequency, the same ion-neutral collision rate coefficient, and the same neutral density model (Banks and Kockarts, 1973) were used.

The comparison between the measured and computed conductivity is, in general, quite good, and confirms the overall validity of the measurement. However, there are some discrepancies which are significant and have to be resolved. The measured Hall conductivity is somewhat smaller than predicted, the peak Pedersen conductivity is larger than predicted, and there are some alarming excursions into negative conductivity. The most likely explanation of these problems is that the effective conductivity in the earth-fixed frame is being changed by neutral winds.

6. Neutral Wind

The neutral wind velocity may be calculated from measurements of the ion flow velocity and electric field if the conductivity is known or assumed. In equation 2 of their paper, Brekke et al. give an expression for ion velocity involving neutral wind which may be solved for neutral wind as a function of ion flow and electric field.

$$\bar{u} = \bar{v}_i - \frac{\Omega_i}{\nu_{in} B} \left(\bar{E} + \bar{v}_i \times \bar{B} \right) \qquad (3)$$

where $\bar{u}$ is the neutral wind velocity and Ω_i is the ion cyclotron frequency. Using the same values for Ω_i and ν_{in} that were used

above to compute the model conductivity profiles, the neutral wind velocity has been calculated from the SNT 7/1 data. This procedure is equivalent to assuming the conductivity to be equal to the calculated profiles shown in Figure 10. Figure 11 shows the results of these calculations plotted as a function of altitude.

The neutral wind measurements indicate that the winds had somewhat high velocities and exhibited substantial altitude variation at the time of this flight. The north - south component rises from small values below 100 km to around 300 - 350 m/sec southward above 110 km. The west - east component varies substantially with altitude. It ranges from small values at high altitudes to 350 m/sec westward at 117 km and then reverses to 200 m/sec eastward at 105 km. At lower altitudes, the situation is obscured by rapidly increasing systematic errors, but the wind appears to become westward again. Generally similar comments to those made above can be made about the relative size and importance of statistical and systematic errors. It should be noted that the relative size of the systematic errors appears to be somewhat larger in the neutral wind results than in the other results, and grows rapidly at the lower altitudes. The size of all errors grows rapidly above 135 km.

This is the first in situ point measurement of neutral winds ever made in the winter midnight auroral zone ionosphere making direct comparison with other data impossible. All of the other high altitude neutral wind measurement techniques either cannot be used in such circumstances, or do not make point measurements. The most commonly used technique, optical tracking of artificially introduced gas clouds (Smith, 1968; Rees, 1971; Stoffregen et al., 1972; Stoffregen, 1972; Meriwether et al., 1973), requires that the cloud be in sunlight, a condition impossible to fulfill at winter midnight in the auroral

zone. None of the other three techniques--measurement of the Doppler shift in irglow emission lines (Hays and Roble, 1971), measurement of satellite drag (De Vries, 1972) or incoherent scatter radar measurements of ion flow velocities in the E and F regions (Brekke et al., 1973)--make point measurements.

Despite the impossibility of a direct comparison, qualitative comparison of these results with the previous work cited above is still of interest. The range of magnitude and direction that have been reported at high latitude is enormous. The highest velocity measured, by De Vries, was 1000 m/sec. Roughly half of the results cited reported winds of 300 m/sec or more. There appeared to be a correlation of high velocities with magnetic activity, with proximity to the auroral zone, and with proximity to the midnight sector. Those authors who did show point measurement profiles from the auroral zone during aurora (Smith, Rees) reported profiles that were qualitatively similar to the results reported here in terms of variation with altitude. It seems, therefore, that the results shown in Figure 11 are in reasonable agreement with previous results and are a valid measurement of neutral wind velocity.

D. Difference Current Measurements at Large Negative Potentials--Ion Flow Measurements: Results from SNT 7/2

1. Methods of Data Analysis

The methods used for analyzing the SNT 7/2 data were, in general, exactly the same as those used for SNT 7/1. There were some differences engendered by the noise problem discussed above. First, there was substantially more analog filtering used before passing the signal to the PCM decoder. Second, the criterion for synchronization used in preparing synch word checked tapes in the computer (Schutz, 1973) was relaxed

somewhat in order to facilitate correcting the timing on the final digital tapes. Finally, the sine wave fit procedure was monitored in detail in real time on a VISTA console, adjustments made in the control parameters as required, and spurious fits rejected from the output selected for final analysis.

The analysis procedure was also altered somewhat by the fact that the parallel detector worked. The various DC offsets affecting the parallel detector, discussed in Chapter III, were determined from the data by assuming that the ambient flow was constant or nearly so from one sweep to the next. The DC offsets were then solved for algebraicly at each probe input relay change and motor rotation. Since the assumption is somewhat questionable, this procedure is most accurate when the results are averaged over a large body of data centered on apogee. The noise problem made this impossible, and the accuracy of the resulting DC offset corrections is questionable.

2. Parallel Flow

Since the parallel probe data was not completely reliable, it was also necessary to determine the parallel ion velocity using the precession analysis method described above in Chapter IV, and in section C.1 of this chapter. The electric field components deduced from the SNT 7/2 data for various assumptions of v_B appear in Figure 13. The choice of v_B that is required to minimize the apparent precession periodicity in the results prior to t = 130 seconds is 1.6 km/second. This result is plotted in the bottom panel of Figure 14 along with the velocity deduced from the parallel probe data, and with other possible assumptions as discussed above in regard to the 7/1 analysis. There is a substantial difference between the probe data and the results of the precession analysis. Because of the problems

with the DC offset corrections, the precession analysis result is believed to be more reliable.

Comparison of the bottom panels of Figures 7 and 14 indicate that the SNT 7/2 parallel flow data appears to be a more or less smooth continuation of the 7/1 results into the lower upleg region where no data was obtained on 7/1. This continuation is a remarkable coincidence, considering the difference in geophysical conditions. It is, in fact, no coincidence but rather a manifestation of the same rocket-plasma interaction effect discussed in section C. 2 of this chapter.

3. Perpendicular Flow

There are several problems one encounters in the perpendicular flow analysis that are difficult to resolve without the opportunity to compare the split and double probe results above 140 km. They include choosing the best parallel flow analysis result, deciding whether or not to use the wake correction, checking the accuracy of the focusing model, and checking for any human errors in experiment installation. These possible problems, and the difficulty in resolving them, reduce the overall confidence in the results of the perpendicular flow measurement and subsequent analyses. Under the assumptions that no human blunders were made in preparing the payload, and that it is most appropriate to do so, the same analysis procedures and parameters have been employed for SNT 7/2 as for 7/1.

In addition to these methodological difficulties associated with the lack of data at apogee, the early upleg data from probe experiments may be subject to systematic errors of unknown magnitude due to various "settling down" effects. These are hypothetical effects caused by outgassing and other adjustments to the space environment (Haerendel, et al., 1974). The possi-

bility that these effects have perturbed the data also reduces confidence in the 7/2 perpendicular flow results.

Despite these reservations, the quality of the noise-filtered 7/2 data that does exist appears to be as good as the 7/1 data. No reason to doubt the validity of the 7/1 analysis choices as applied to the 7/2 data has arisen. All of the analyses have been carried through to completion, and the results merit serious consideration.

The perpendicular flow data from the 7/2 flight appear in Figure 15, using the best fit precession analysis parallel velocity value as shown in the bottom panel. As above, the electric fields measured by Ulf Fahleson's double probe experiment and transmitted via the split Langmuir probe's PCM telemetry system are also shown. Once again, there are differences between the two measurements which appear to be due to the effect of ion-neutral collisions on ion mobility and which can be translated into a measurement of current density.

4. Current Density

The current density has been determined from the SNT 7/2 data using the same method as was used for the 7/1 data. The results are shown in Figure 16, along with selected points from the other analyses shown in Figure 14. The same comments about the relative size and importance of statistical and systematic errors can be made about these results as about the 7/1 results, keeping in mind that the scatter in the results of the various analyses might represent somewhat of an underestimate of the systematic errors on this flight.

On the upleg, the rocket passed through a north-east current, with a maximum northward current density of 1.85 $\times 10^{-5}$ amperes/meter^2 at 112 km and a maximum eastward

current density of 4.4×10^{-5} amperes/meter^2 at 105 km. The height integrated current up to 140 im was 0.68 amperes/meter, flowing at an azimuth of 55°. On the down leg, the single measurement made showed a current of 4.2×10^{-5} amperes/meter^2 flowing at an azimuth of 229°. These values are roughly comparable with previous measurements as cited in part C.4 of this section.

In comparison, the magnetic disturbance field measured at ESRANGE during the flight was $\Delta x \approx -175\gamma$ decreasing to -125γ, $\Delta y \approx 0$, and $\Delta z \approx -70\gamma$. The measured magnetic disturbance vector implied that the net ionospheric current was westward, with no north-south component. The ionospheric current actually measured by the rocket is not comparable to the current implied by the ground magnetometer data. This disagreement has some very interesting implications about auroral structure which will be discussed below.

5. Conductivity

The Hall and Pedersen conductivities have been calculated from the SNT 7/2 data using the same methods that were used for the 7/1 data. Figure 17 displays these conductivities, plotted as a function of altitude. Again, the same comments about errors apply.

The maximum Hall conductivity on the upleg was 1.43×10^{-3} mho/meter at 105 km. The maximum Pedersen conductivity was 1.32×10^{-3} mho/meter at the same altitude. The height integrated Hall conductivity was 11.7 mho and the height integrated Pedersen conductivity was 23.8 mho. On the down leg, the Hall conductivity at the single point measured was 5.3×10^{-3} mho/meter and the Pedersen conductivity was 5.0×10^{-3} mho/meter.

Model conductivity profiles for the SNT 7/2 flight were calculated using exactly the same technique that was used for the 7/1 flight. These profiles are also plotted in Figure 17. There are substantial discrepancies between the data and the model. These differences are probably due to changes in the effective conductivity in the earth-fixed frame caused by the presence of neutral winds.

6. Neutral Winds

The neutral wind velocity has been deduced from the SNT 7/2 data using the same method that was used for 7/1. The wind velocity is plotted in Figure 18 as a function of altitude.

The scatter in the results from the various analyses is much larger in Figure 18 than in Figure 11. This implies that the systematic errors are relatively larger in the 7/2 neutral wind measurements than in the 7/1 measurements. In particular, the data below 95 km shows a much larger wind velocity than has previously been reported for this altitude range, which could be a manifestation of the "settling down" effects mentioned above.

These measurements indicate that the winds were blowing in a north to northwest direction on the upleg, with northward velocities of about 300-500 meters/second at all altitudes. The westward velocity is small or zero below 115 km and increases to around 350 meters/second above that. The downleg wind was southwestward, at about 400 meters/second. Since the trajectory was northward, the wind configuration was quite remarkable. Its implications are discussed in the next section.

E. Discussion

It is profitless and impossible to discuss the electric field, current density, and conductivity results from the flight of SNT 7/1 further until the data from the other experiments has been analyzed.

A generally similar statement can be made about the results from the SNT 7/2 flight. However, some comments can be made about the implications of the current density measurements. As reported, the rocket measurements did not agree with the ground magnetometer results. The measurement of strong northward and southward components on the up and downlegs respectively, when contrasted with the ground measurement of no east-west magnetic disturbances, suggest that the rocket passed through a current configuration similar to that proposed by Boström (1968) and seen previously by Park and Cloutier (1971), Cloutier et al. (1973) and possibly also on the Javelin flight discussed above. This configuration is one where the north-south currents flow only across the regions of enhanced conductivity associated with arcs, and are connected to the deep magnetosphere by east-west oriented Birkeland sheet currents of substantial extent, thus forming solenoid-like configurations which cause little net external field change.

The measurement of eastward current on the upleg and net westward current from the ground implies that there were at least two electrojets present--one eastward and a stronger one westward. The fact that the aurora displayed several parallel arcs as shown in Figure 3 suggests the hypothesis that the total current configuration was composed of several alternating east and west electrojects associated with several alternating up and down Birkeland currents. A similar configuration was reported by Cloutier et al. (1973). A more

detailed investigation of this hypothesis will be possible after the completion of the analysis of data from the other experiments on the rocket.

It is difficult to discuss isolated neutral wind measurements without more extensive information about the surrounding meteorological circumstances than is available. Nonetheless, there are a few statements which can be made. First, the measurements of neutral wind reported here are substantially higher than any measured in the midnight sector by Brekke et al. using the Chatanika radar. Since the analyses performed here were done in such a way as to insure maximum comparibility, this is curious. It should be noted that the radar results represent both a temporal and a spatial average of the data. Since other point measurements, such as those reported by Smith, Rees, Stoffregen et al., and Meriwether et al., also give higher velocity results than Brekke et al., something may be wrong with their procedure. In view of the substantial altitude variation shown in Figures 28 and 35, the problem may be associated with the height averaging required by their method.

The results reported here also have some implications about the forces which drive high latitude, high altitude neutral winds. Historically, the main forces that have been included in theoretical studies of these winds were solar heating, tides, and inertia (Rishbeth, 1972). Recently, wind data from the auroral zone and polar cap and from periods of magnetic storms (see the papers cited above) has become available, and has not agreed with such models. Two hypotheses have been advanced to explain the disagreement. One hypothesis is that the anomalies are due to pressure forces created by heating of the ionosphere by the aurora (Stoffregen, 1972). The other hypothesis is that the discrepancies are due to ion drag forces and

electric field (Fedder and Banks, 1972; Meriwether et al., 1973). The data shown in Figure 11 and 18 are not in agreement with model predictions given by Rishbeth. Presumably, this was caused by one or both of these forces.

The winds measured on the 7/1 flight could have been driven by either force, although the large westward component argues somewhat in favor of the ion drag model. The winds detected on the 7/2 flight could not have been caused by pressure gradient forces. The winds shown in Figure 18 are directed at the arc, not away from it as predicted by the heating model. In fact, the winds are oriented so as to contribute to building up the pressure ridge under the arc. This interesting configuration appears to have come about because the aurora was relatively steady for 1 $\frac{1}{2}$ to 2 hours before the flight. This was sufficient time, according to the calculations of Fedder and Banks, for the highly structured local electric fields to substantially alter neutral wind patterns down to as low as 100-110 km.

IV. Experiment Design Details -- Swedish Nike Tomahawk 7 Instrument

A. The Probe

The decision to use probes that were as small as possible, which was made after the first flight, represented a substantial mechanical design challenge. The problem of designing a probe that was small compared to the Debye length, strong enough to withstand the stresses of launch, spin-up and deployment, and which could be fabricated with the required area accuracy was extremely formidable. Compounding the problem was the requirement that the detecting surfaces be covered with aquadag with the same area accuracy and without the aquadag ever being touched.

The solution ultimately employed on the Swedish rockets is shown in Figure 19. The charge collector plates were precision ground tungsten plates. These were glued as shown to a less precise substrate, and then were coated with aquadag by hand painting under a microscope. This approach produced the required strength and area accuracy. However, a certain amount of tungsten was left bare of aquadag. This was the major compromise in the design.

B. The Electronics

The major electronic design challenge posed by this instrument was the necessity of measuring a difference between two probe currents that might be as small as one part in 10^4. A block diagram of the resulting circuit is shown in Figure 20. The input stage in the probe circuit was, of course, the most critical. The input operational amplifiers had to meet quite

severe specifications. The common mode rejection ratio had to be greater than 80 db at 4 Hz, and the bias current had to be less than the smallest difference current that it was desired to detect, 5×10^{-13} amperes. In addition, the offset voltage had to be trimmable without increasing the bias current significantly. Finally, the slew rate had to be fast enough and the parasitic capacitance small enough so that the output settled to within one part in 10^4 of its final value faster than the telemetry system could respond using the maximum feedback resistance. This was not easy to do. The amplifiers finally used, Intech A-125, met the specifications, but had the disadvantage of being quite large (see Figure 22) and expensive.

Obtaining the required dynamic range at the output of these amplifiers was also a problem. The possibility of using a logarithmic circuit with a diode feedback element was explored, but it proved impossible to obtain matched elements which were matched with sufficient accuracy. The solution used was a set of 8 feedback resistors, which were switched in and out of use by mechanical relays driven by an automatic gain control circuit. The most important specification on the resistors (RO-7 A & B in Figure 21) was that they be matched to within one part in 10^4. Matched resistor pairs of this accuracy are available commercially up to 20 MΩ. Use of a high precision 5 place digital ohmmeter made it possible to trim the resistor pairs less than 10 MΩ to within 5 parts in 10^5.

The requirements of the circuit also placed special constraints on the relays used to switch in the resistors. Parasitic capacitances had to be as small as possible, leakage resistance had to be greater than 3×10^{11} Ω and the close

and bounce time had to be less than 3 milliseconds. As it turned out, only one available relay with the necessary speed and lack of bounce also had the high leakage resistance required.

Also on the input cards were comparators which took the difference between input currents and which subtracted the sweep voltage.

In addition to the split probes, the instrument had two other probes attached to it. First, there was the so-called Δn experiment shown in Figure 21. This device is the work of another experimentor in the Space Sciences Laboratory and is outside the scope of this thesis. Second, there was the V_{G1} probe. This was an unloaded axis-symmetric probe used to provide a stable reference voltage for the sweep. As can be seen in the interconnection diagram (Figure 20), this voltage was sensed, low pass filtered, and added to the sweep voltage on the Gain State Card (Figure 23).

Also on the Gain State Card was the automatic gain control circuitry which sensed the output voltage of the single plate current comparator and adjusted the feedback resistance up or down if the voltage was outside set limits. Note that different gain comparators were sensed depending on whether the current was positive or negative.

The logic of the gain control circuits was arranged so that the gain could change one step per telemetry word only. It could change every word as long as it continued to increase or decrease monotonically. To change direction, it had to wait two words unless it was in the highest or lowest states possible.

The last circuit on the Gain State Card was a sample and hold and a multiplexer which sequenced the data into the analog to digital converter shown in Figure 24. The multiplexer and sample and hold are driven by the main programmer card,

shown in Figure 25, which also drives the A-D converter, the pulse code modulation encoder and readout, the sweep generator, and the parallel probe spin motor controller.

The readout card, shown in Figure 26, takes the various quantities passed to it by the ADC and programmer cards and assembles them into a 16 kHz pulse code modulated (PCM) signal for transmission to the telemetry system of the rocket. The PCM signal was transmitted to ground on FM-FM telemetry subcarrier channel H. The main reason for this complex procedure was to achieve large dynamic range in the difference current channels without absorbing too many telemetry channels. This was achieved by using a 12 bit PCM format (see Figure 28) and by changing gain every two frames if necessary. The 6 millisecond frame interval of the PCM telemetry, which was set by the bandwidth of Channel H, in turn established the basic performance requirements imposed on the input relays and operational amplifiers.

Figure 27 shows the details of the last card in the box, the motor controller card. This card accomplished two major functions. First, a suitably programmed digital to analog converter generated the sweep. Second, drive circuitry controlled a stepping motor which rapidly reversed the orientation of the parallel probe at the start of every fourth sweep. This was done to determine the values of any DC offsets which the probe had.

The circuits of the two main pieces of ground support equipment are shown in Figures 29 and 30.

References

Banks, P.M. and G. Kockarts, Aeronomy, Academic, New York, 1973.

Bering, E.A., Auroral zone electric current measurements on sounding rockets, Ph.D. thesis, University of California, Berkeley, 1974.

Bering, E.A., M.C. Kelley and F.S. Mozer, Split Langmuir probe measurements of current density and electric fields in an aurora, J. Geophys. Res., 78, 2201, 1973.

Boström, R., A model of the auroral electrojet, J. Geophys. Res., 69, 4983, 1964.

Boström, R., Currents in the ionosphere and magnetosphere, Ann. Geophys., 24, 681, 1968.

Brekke, A., J.R. Coupnik and P.M. Banks, A preliminary study of the neutral wind in the auroral E region, J. Geophys. Res., 78, 8235, 1973.

Cloutier, P.A., B.R. Sandel, H.R. Anderson, P.M. Pazich, and R.J. Spiger, Measurement of auroral Birkeland currents and energetic particle fluxes, J. Geophys. Res., 78, 640, 1973.

DeVries, L.L., Structure and motion of the thermosphere shown by density data from the low-G accelerometer calibration system (LOGACS), Space Res., 12, 867, 1972.

Fedder, J.A. and P.M. Banks, Convection electric fields and polar thermospheric winds, J. Geophys. Res., 77, 2328, 1972.

Haerendel, G., H. Kappler, M.C. Kelley, F.S. Mozer and U.V. Fahleson, Electric field measurements in a major magnetospheric substorm, J. Geophys. Res., (submitted), 1974.

Hays, P.G. and R.G. Robel, Direct observations of thermospheric winds during geomagneti storms, J. Geophys. Res., 76 5316, 1971.

Kelley, M.C., Auroral zone electric field measurements on sounding rockets, Ph.D. Thesis, University of California, Berkeley, 1970.

Meriwether, J.W., J.P. Heppner, J.D. Stolarik and E.M. Wescott, Neutral winds above 200 km at high latitudes, J. Geophys. Res., 78, 6643, 1973.

Park, R.J. and P.A. Cloutier, Rocket based measurements of Birkeland currents in an auroral arc and electrojet, J. Geophys. Res., 76, 7714, 1971.

Rees, D., Ionospheric winds in the auroral zone, J. Brit. Interplanet. Soc., 24, 233, 1971.

Rishbeth, H., Thermospheric winds and the F-region: A review, J. Atmos. Terr. Phys., 34, 1, 1972.

Schutz, S.R., Rocket measurements of electric fields in the mid-latitude ionosphere, Ph.D. Thesis, University of California, Berkeley, 1973.

Smith, L. B., An observation of strong thermospheric winds during a geomagnetic storm, J. Geophys. Res., 73, 4959, 1968.

Stoffregen, W., The anomaly of the neutral wind at a height of ≃ 200 km at high latitudes, in Magnetosphere-Ionosphere Interactions, ed. K. Folkestad, p. 83, Universitetsforlaget, Oslo, Norway, 1972.

Stoffregen, W., H. Derblom, L. Ladell and H. Gunnarsson, The chemistry of artificial clouds in the upper atmosphere and their response to winds and fields, Uppsala Jonosfärobervatorium Report 17, Part B, 1971.

TABLE I

PROBE GEOMETRY

FLIGHT	PROBE CONFIGURATION	PROBE DIMENSIONS	BOOM LENGTH	REMARKS
Javelin 8.56	Cylinder	Diameter = 3mm Length = 9.5 mm & two 14 mm long guard cylinders	$\sim\frac{1}{2}$ m	
Swedish Nike Tomahawk 7/1 & 2	Rectangular Prism	Width = 5 mm Length = 10 cm Thickness = 3.8 mm & two 2.54 cm guard sections	$\sim\frac{1}{2}$ m	Parallel Probe motor mounted

TABLE II

SWEEP CHARACTERISTICS

FLIGHT	PROBE	WAVEFORM	PERIOD(S)	VOLTAGES
Javelin 8.56	Parallel	"	1 second	12 volts
	Perpendicular	"	0.1 seconds	12 volts
Swedish Nike Tomahawk 7/1	Parallel	Stepped Ramp	6.3 seconds overall 3 step pattern step widths = .79 sec., 4.7 sec., .79 sec.,	2 volt ramp centered on + 1.7 steps are 3 volts (sweep goes from -2.3 to +5.7 volts)
	Perpendicular	"		
Swedish Nike Tomahawk 7/2	Parallel	"	6.3 sec. overall 2 step pattern step widths = .79 sec., 5.5 sec.	2 volt ramp step is 2.5 volts (sweep goes from -2.3 to +2.0 volts)
	Perpendicular	"		

Figure Captions

Figure 1: Artist's conception of the SNT 7 payload just after deployment. (Figure courtesy of SAAB).

Figure 2: Magnetogram from ESRANGE, Kiruna, Sweden for the night of 7-8 February, 1972. Dashed line shows time of launch of SNT 7/1.

Figure 3: "All-Sky" Camera photograph taken from Jukkasjärvi, Sweden at 00 56 UT on 9 February 1973, showing auroral arcs penetrated by rocket SNT 7/2.

Figure 4: Magnetogram from ESRANGE, Kiruna, Sweden for the night of 8-9 February, 1973. Dashed line shows time of launch of SNT 7/2. Figure 1 was taken 2 minutes later.

Figure 5: Plasma density measured by the Uppsala Ionospheric Observatory experiments on SNT 7/1. (Data supplied by B. Holback, UJO)

Figure 6: Perpendicular components of the electric field measured by the split Langmuir probe on SNT 7/1 deduced using various assumptions on the parallel ion flow velocity in the earth-fixed frame of reference.

Figure 7: Perpendicular electric field components in the earth fixed geomagnetic north and west directions, and parallel ion flow velocity in the earth-fixed frame. Four sets of curves are plotted for the electric field, showing field values deduced for three assumptions of parallel flow and field values deduced from ion flow data "corrected" by subtracting $\sqrt{m_e/m_i}$ times the apparent electron flow data. (SNT 7/1 data)

Figure 8: Perpendicular electric field components in the earth-fixed geomagnetic north and west directions, measured by the split Langmuir probe and by the double probe detectors on SNT 7/1; and parallel ion flow velocity in the earth-fixed frame measured by the split Langmuir probe. The split Langmuir probe analysis was done assuming the values of v_B as shown. The double probe analysis was done assuming the parallel component of the electric field is zero.

Figure 9: Perpendicular current density components in the earth-fixed geomagnetic north and west directions deduced from the ion flow measured by the split Langmuir probe and from the electron flow deduced from the electric field measured by the double probe detectors on SNT 7/1. The consequences of making alternative assumptions about parallel ion flow and wake corrections are shown for selected altitudes.

Figure 10: Hall and Pedersen conductivity deduced from the current density shown in Figure 26 and the electric field measured by the double probe detectors on SNT 7/1. The solid lines are the conductivity

profiles predicted by the theoretical model of Brekke et al., (1973) using the density data shown in Figure 22. Alternative assumption results are shown as above.

Figure 11: Perpendicular neutral wind components in the earth-fixed geomagnetic north and west directions deduced from the ion flow velocity measured by by the split Langmuir probe, and the electric field measured by the double probe detectors on SNT 7/1. Alternative assumption results are shown as above.

Figure 12; SNT 7/2 plasma density. Details are the same as Figure 22. (Data supplied by B. Holback, UJO)

Figure 13: SNT 7/2 parallel flow precession analysis. Details are the same as Figure 23.

Figure 14: SNT 7/2 perpendicular electric field components. for five different analyses. Details are the same as Figure 24 for four of the sets of curves shown. In addition, a set of curves is plotted showing the field values deduced using the parallel detector data.

Figure 15: SNT 7/2 perpendicular electric field components. Details are the same as Figure 25.

Figure 16: SNT 7/2 perpendicular current density components. Details are the same as Figure 26.

Figure 17: SNT 7/2 Hall and Pedersen conductivities. Details are the same as Figure 27.

Figure 18: SNT 7/2 perpendicular neutral wind components. Details are the same as Figure 28.

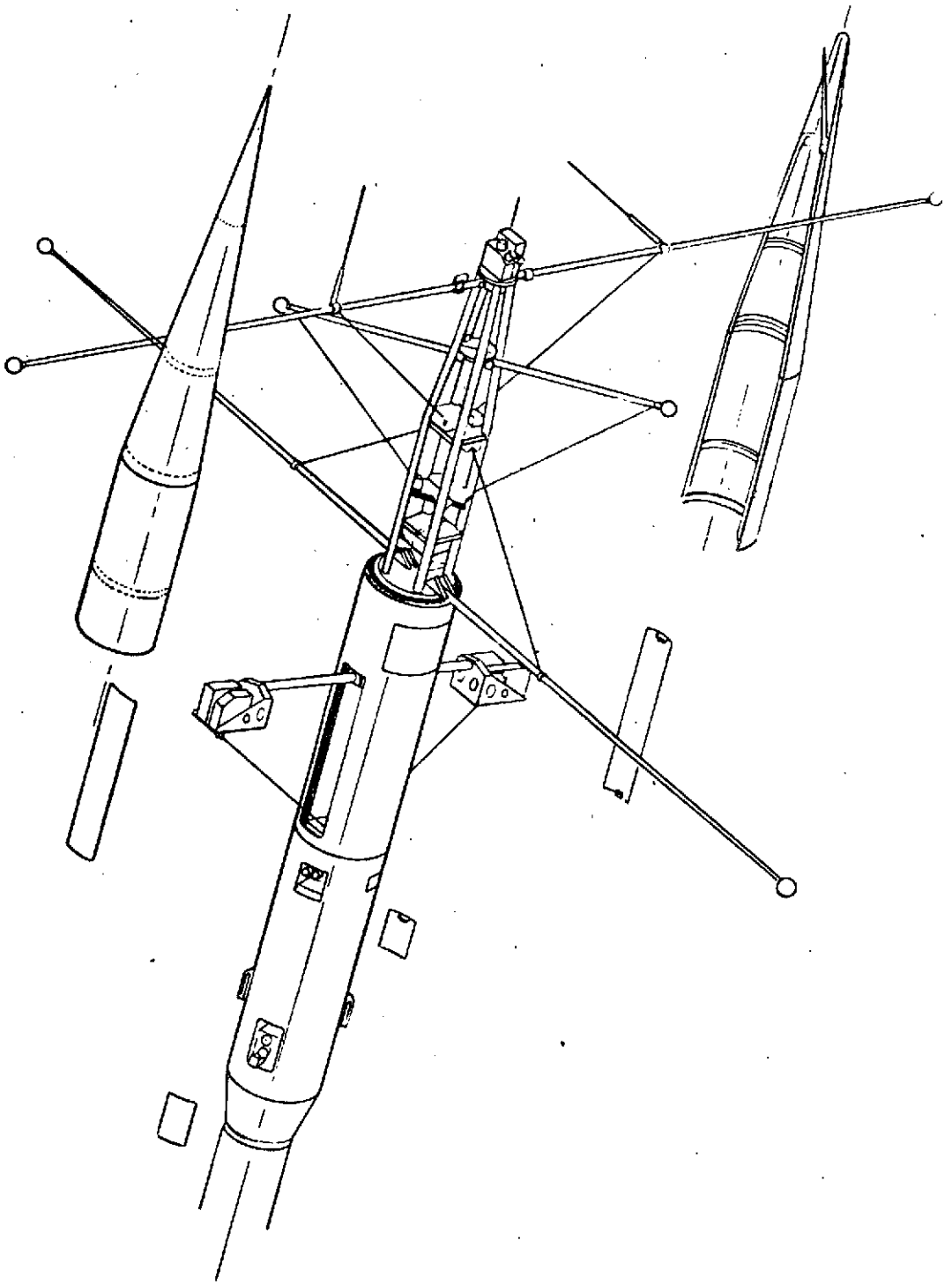

THE SNT 7 AURORAL PAYLOAD DURING THE MEASURING-PHASE

Figure 1

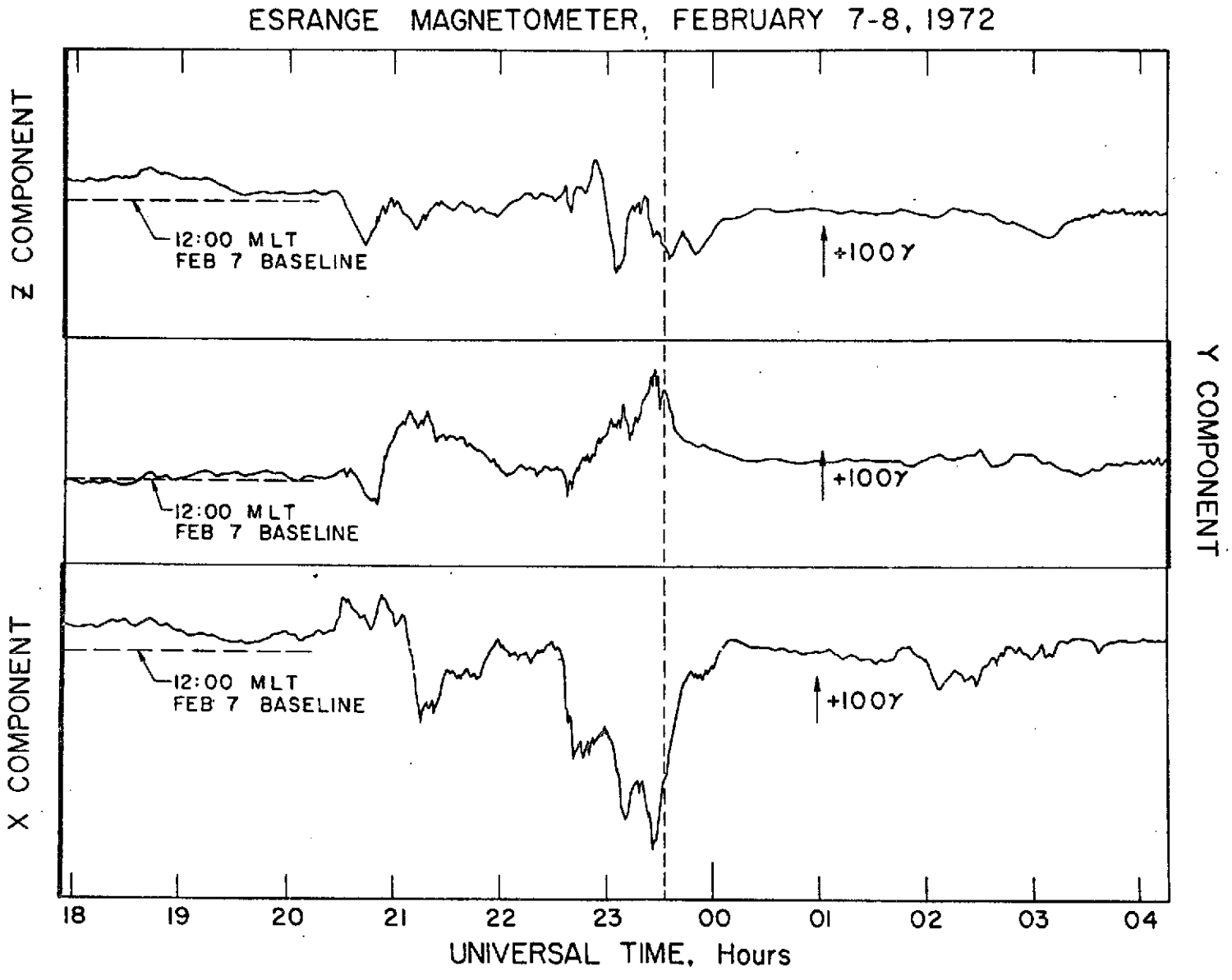
ESRANGE MAGNETOMETER, FEBRUARY 7-8, 1972
Z COMPONENT
12:00 MLT
FEB 7 BASELINE
+100γ
Y COMPONENT
12:00 MLT
FEB 7 BASELINE
+100γ
X COMPONENT
12:00 MLT
FEB 7 BASELINE
+100γ
18
19
20
21
22
23
00
01
02
03
04
UNIVERSAL TIME, Hours

Figure 2

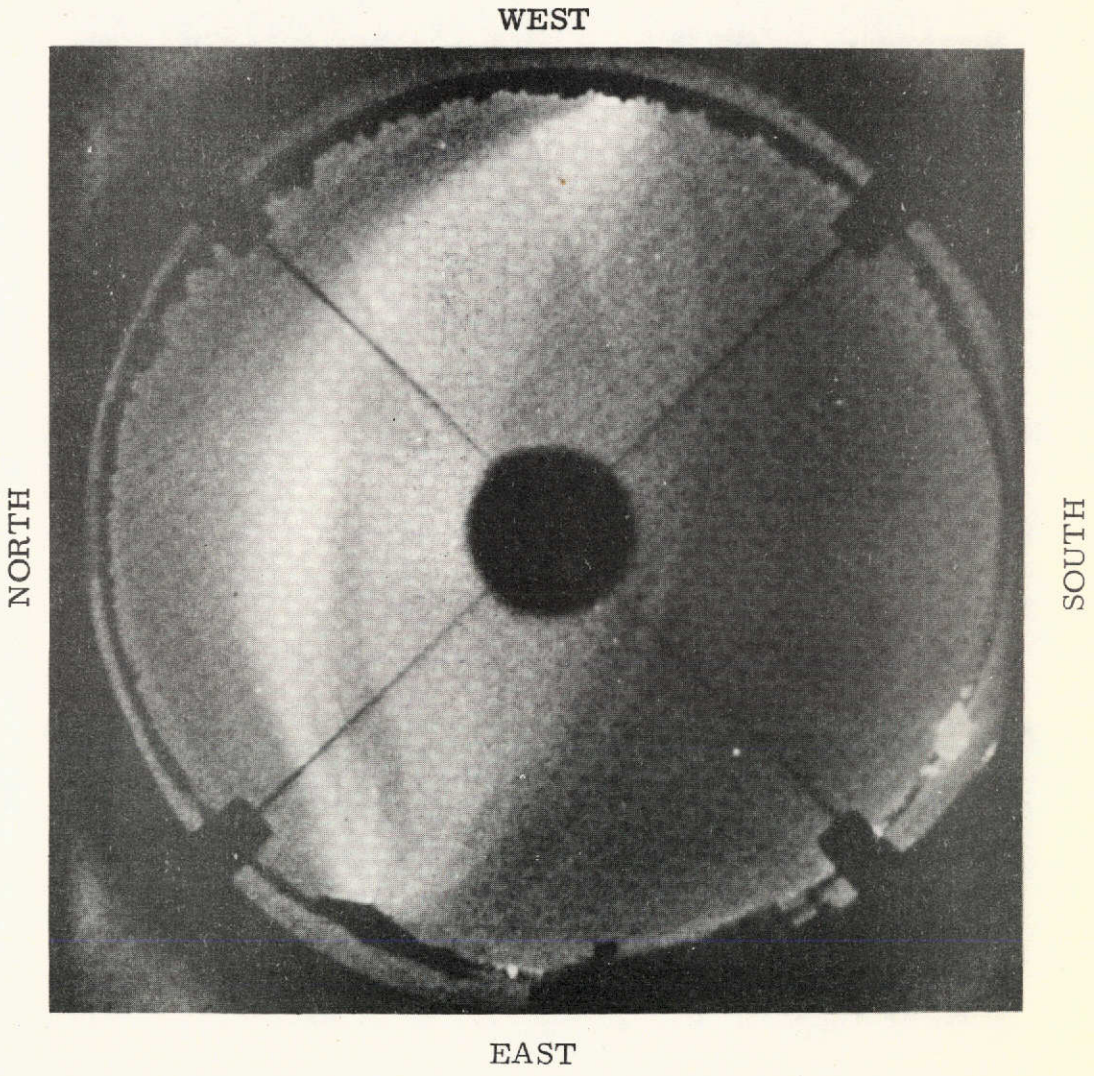

Figure 3

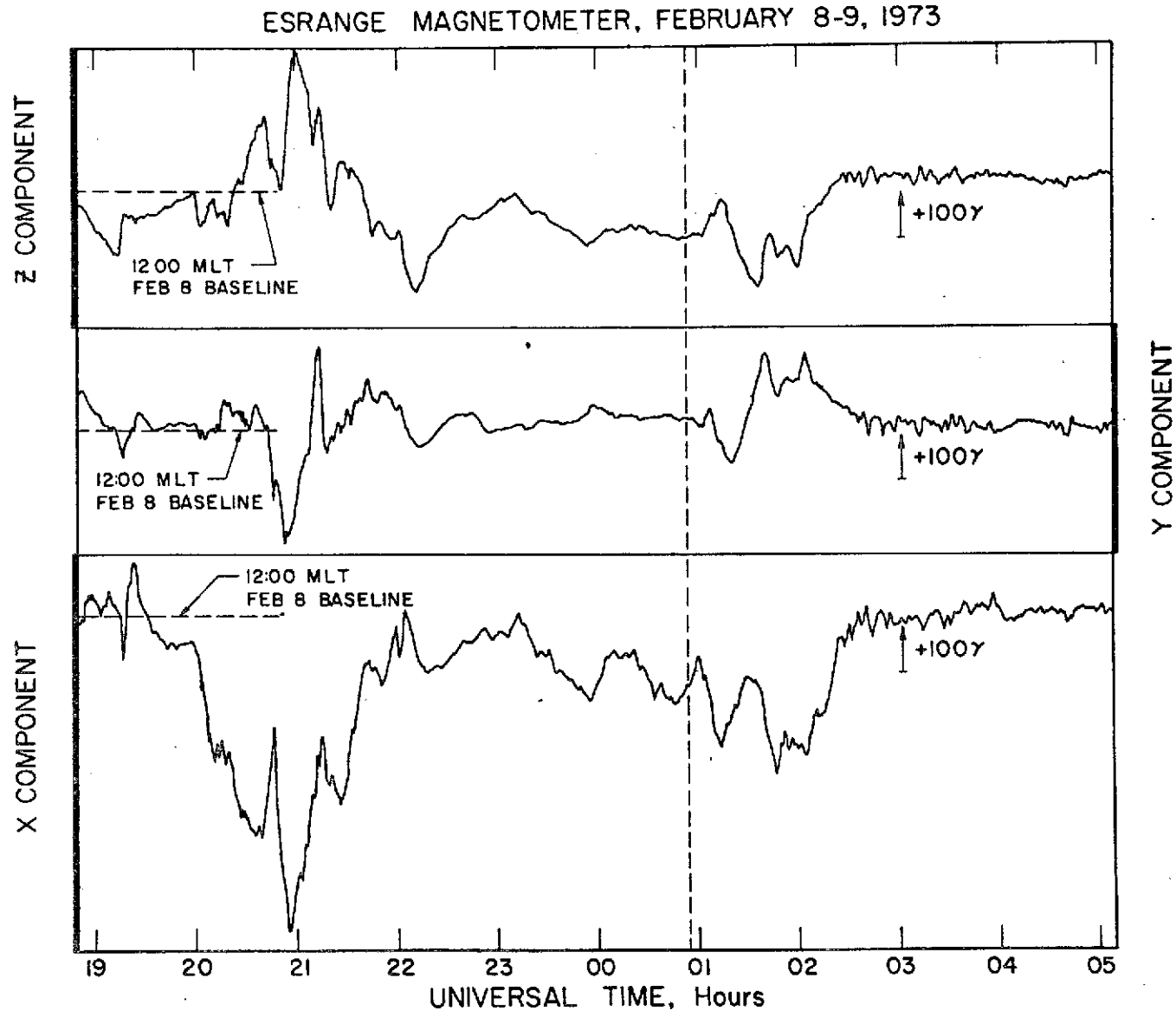
ESRANGE MAGNETOMETER, FEBRUARY 8-9, 1973
Z COMPONENT
12:00 MLT
FEB 8 BASELINE
+100γ
12:00 MLT
FEB 8 BASELINE
+100γ
Y COMPONENT
X COMPONENT
12:00 MLT
FEB 8 BASELINE
+100γ
19
20
21
22
23
00
01
02
03
04
05
UNIVERSAL TIME, Hours

Figure 4

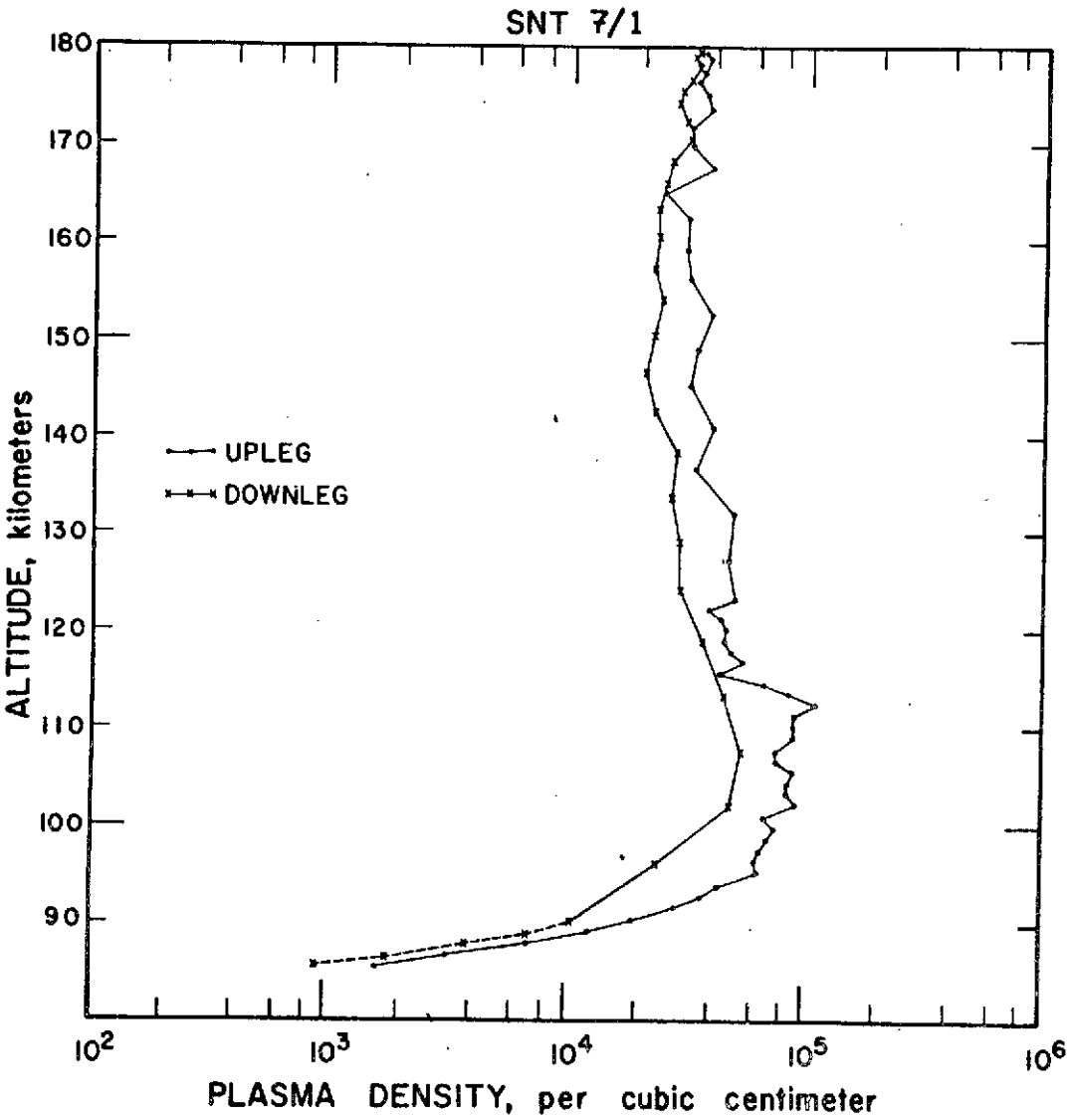
SNT 7/1
180
170
160
150
140
130
120
110
100
90
ALTITUDE, kilometers
UPLEG
DOWNLEG
10^2
10^3
10^4
10^5
10^6
PLASMA DENSITY, per cubic centimeter

Figure 5

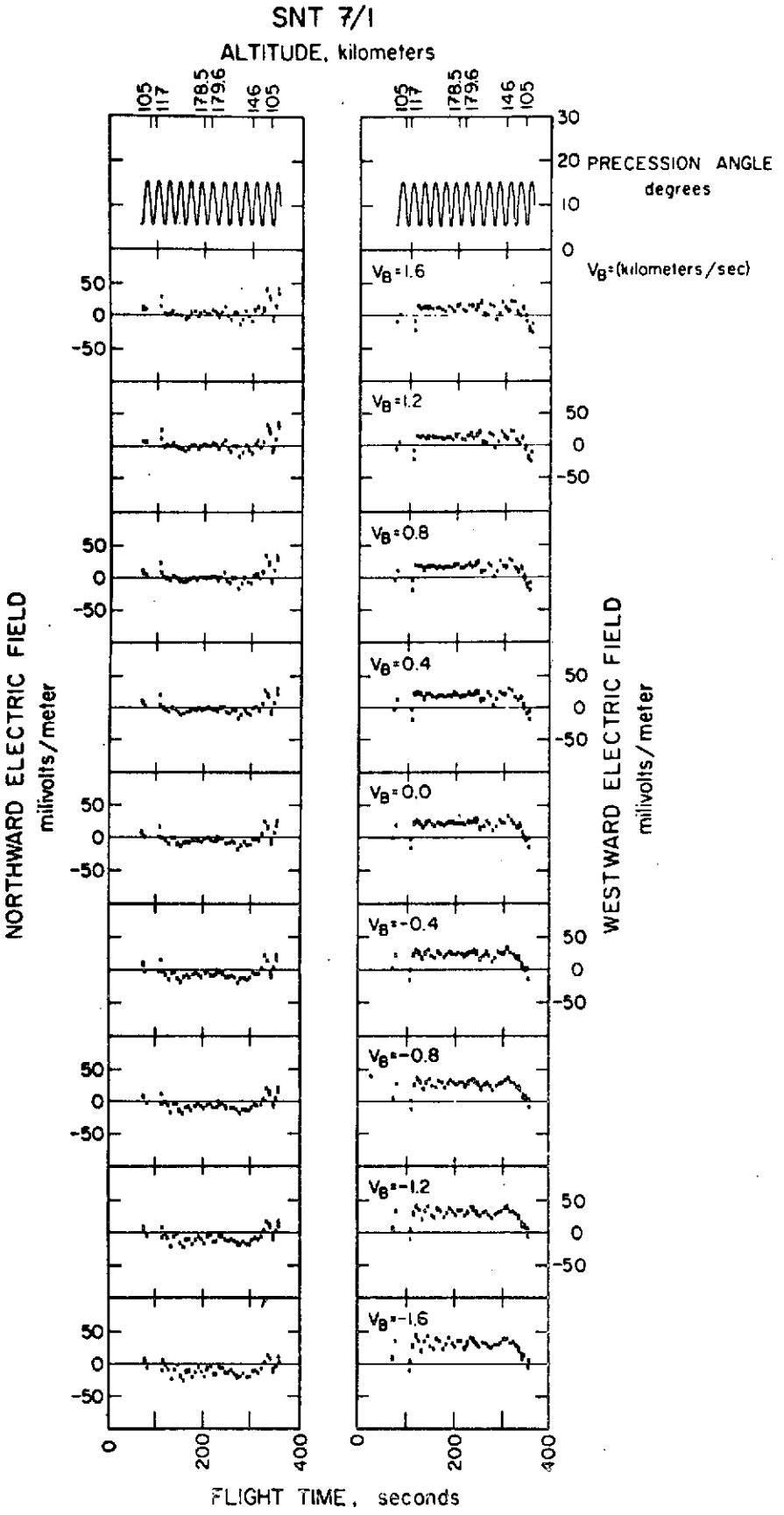
SNT 7/1
ALTITUDE, kilometers
105 117 178.5 179.6 146 105
PRECESSION ANGLE degrees
30
20
10
0
V_B=(kilometers/sec)
V_B=1.6
V_B=1.2
V_B=0.8
V_B=0.4
V_B=0.0
V_B=-0.4
V_B=-0.8
V_B=-1.2
V_B=-1.6
50
0
-50
NORTHWARD ELECTRIC FIELD
milivolts/meter
WESTWARD ELECTRIC FIELD
milivolts/meter
0
200
400
FLIGHT TIME, seconds

Figure 6

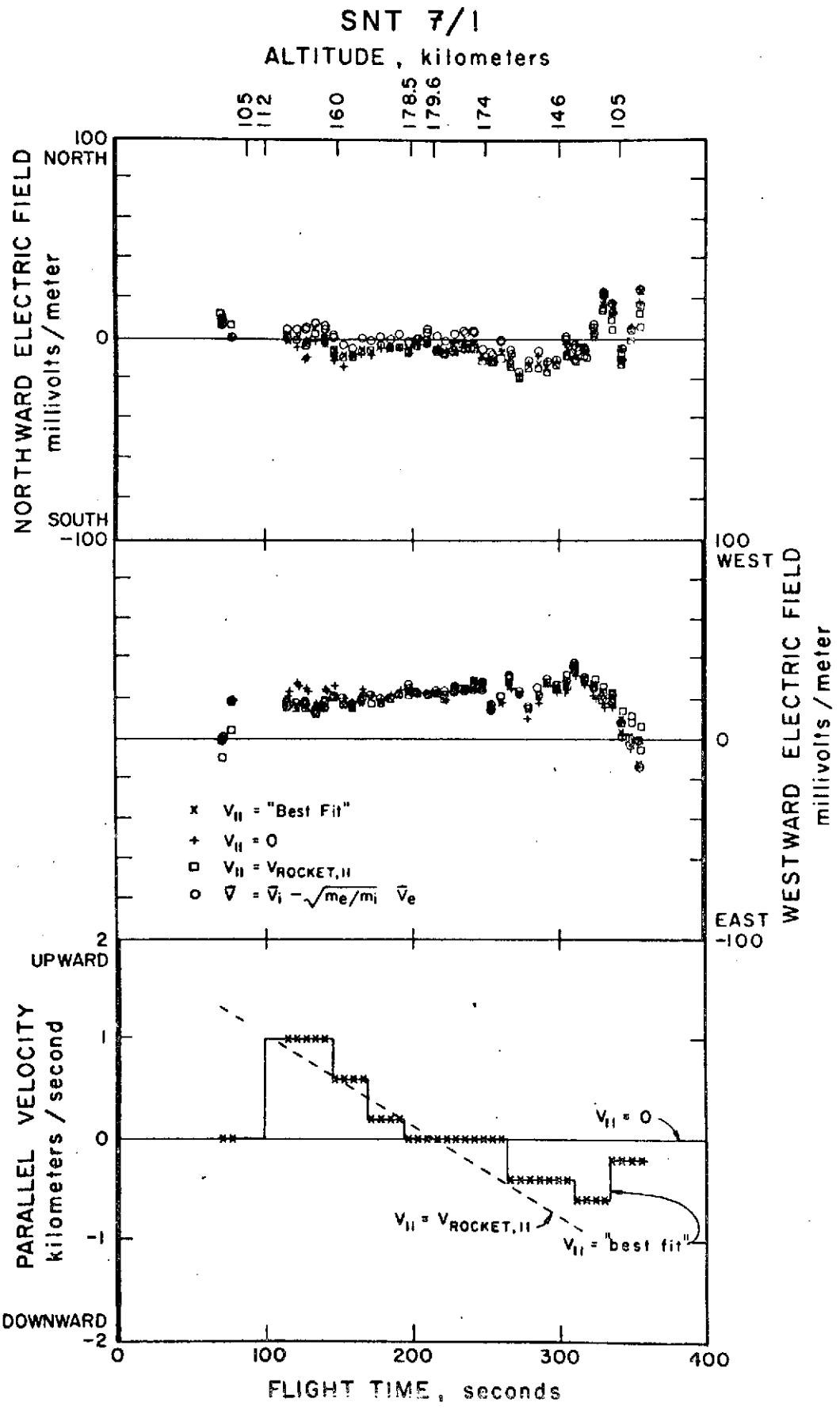
SNT 7/1
ALTITUDE, kilometers
105
112
160
178.5
179.6
174
146
105
NORTHWARD ELECTRIC FIELD
millivolts/meter
100
NORTH
0
SOUTH
-100
WESTWARD ELECTRIC FIELD
millivolts/meter
100
WEST
0
EAST
-100
x $V_{\parallel}$ = "Best Fit"
+ $V_{\parallel} = 0$
□ $V_{\parallel} = V_{ROCKET,\parallel}$
○ $\bar{\nabla} = \bar{v}_i - \sqrt{m_e/m_i}\ \bar{v}_e$
PARALLEL VELOCITY
kilometers/second
2
UPWARD
1
0
-1
DOWNWARD
-2
$V_{\parallel} = 0$
$V_{\parallel} = V_{ROCKET,\parallel}$
$V_{\parallel}$ = "best fit"
0
100
200
300
400
FLIGHT TIME, seconds

Figure 7

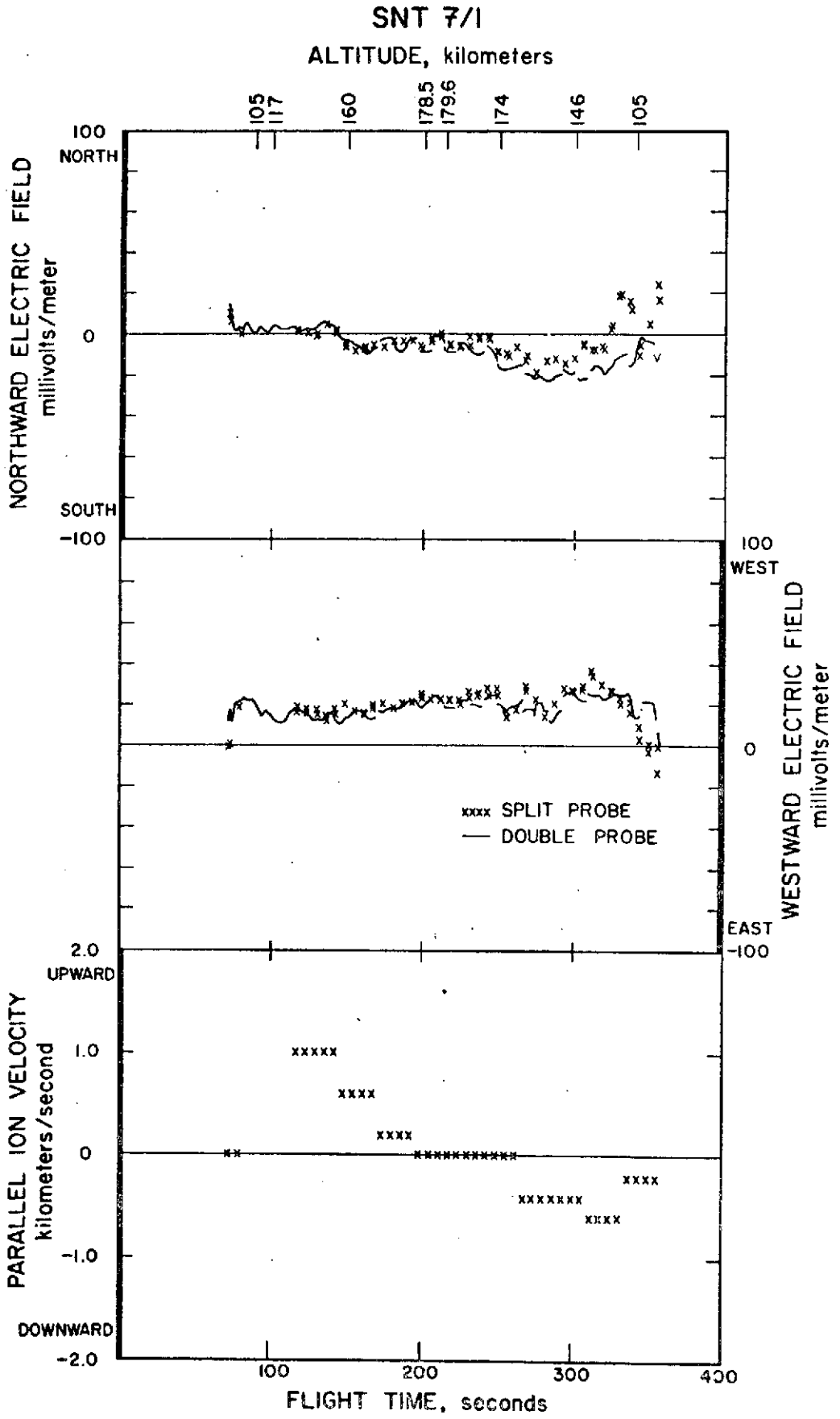
SNT 7/1
ALTITUDE, kilometers
105
117
160
178.5
179.6
174
146
105
100
NORTH
0
SOUTH
-100
NORTHWARD ELECTRIC FIELD
millivolts/meter
100
WEST
0
EAST
-100
WESTWARD ELECTRIC FIELD
millivolts/meter
xxxx SPLIT PROBE
— DOUBLE PROBE
2.0
UPWARD
1.0
0
-1.0
DOWNWARD
-2.0
PARALLEL ION VELOCITY
kilometers/second
100
200
300
400
FLIGHT TIME, seconds

Figure 8

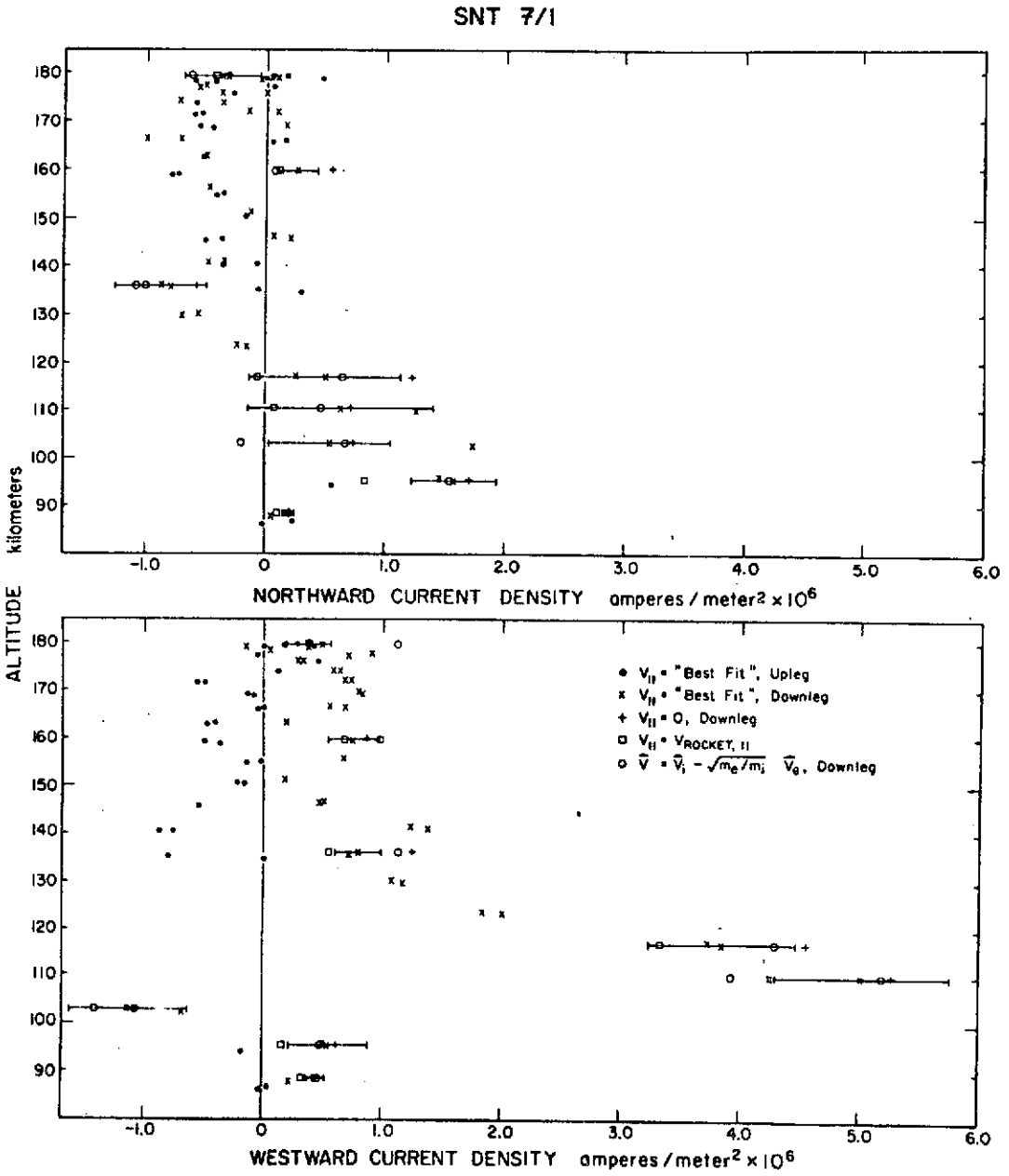
SNT 7/1
ALTITUDE kilometers
NORTHWARD CURRENT DENSITY amperes / meter² x 10⁶
WESTWARD CURRENT DENSITY amperes / meter² x 10⁶
• V_{ii} = "Best Fit", Upleg
× V_{ii} = "Best Fit", Downleg
+ V_{ii} = 0, Downleg
□ V_{ii} = $V_{ROCKET,\,ii}$
○ $\bar{V} = \bar{V}_i - \sqrt{m_e/m_i}\ \bar{V}_e$, Downleg

Figure 9

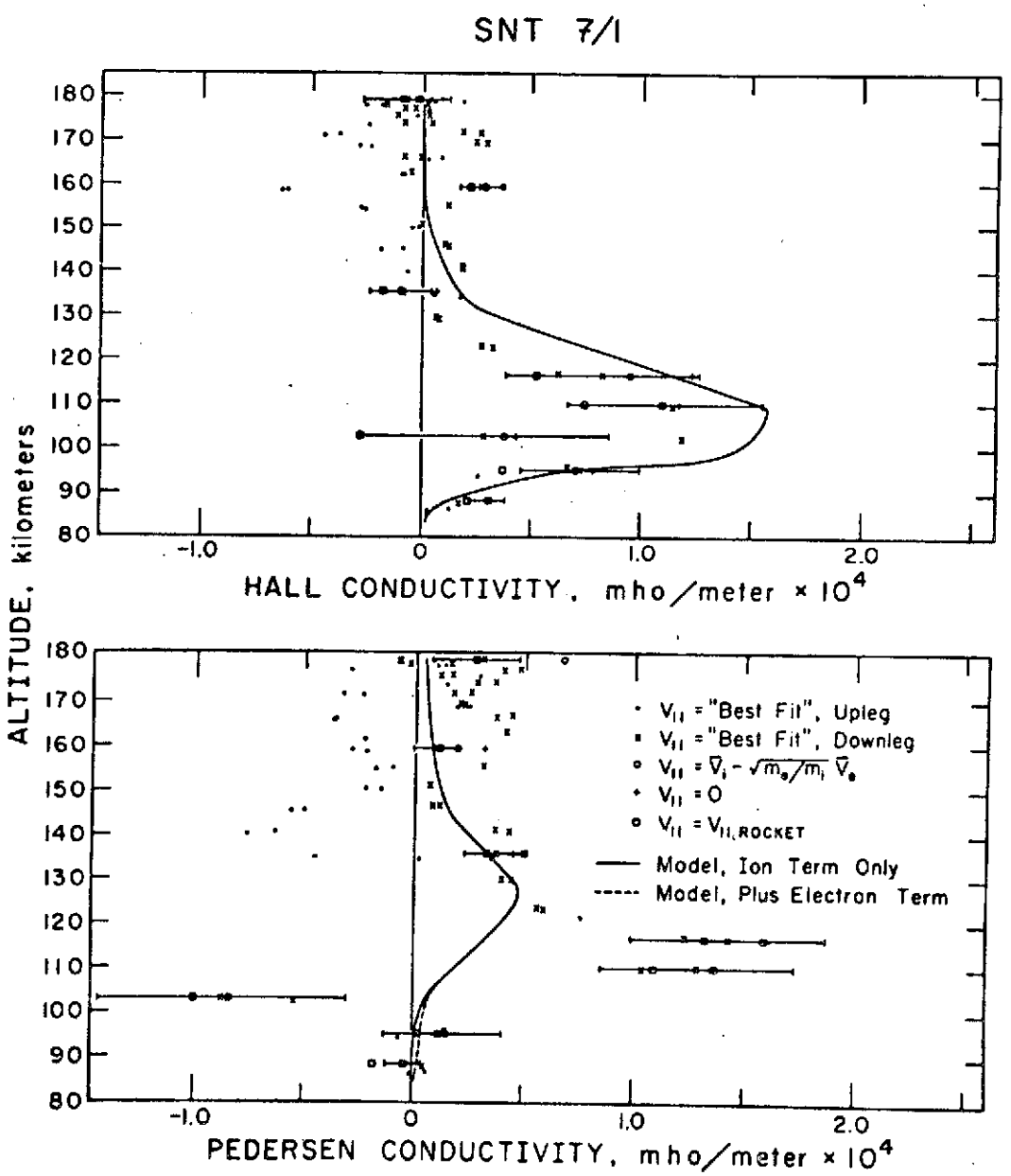
SNT 7/1
ALTITUDE, kilometers
180
170
160
150
140
130
120
110
100
90
80
-1.0
0
1.0
2.0
HALL CONDUCTIVITY, mho/meter × 10⁴
PEDERSEN CONDUCTIVITY, mho/meter × 10⁴
V⊥ = "Best Fit", Upleg
V⊥ = "Best Fit", Downleg
V⊥ = V̄i - √(me/mi) V̄e
V⊥ = 0
V⊥ = V⊥,ROCKET
Model, Ion Term Only
Model, Plus Electron Term

Figure 10

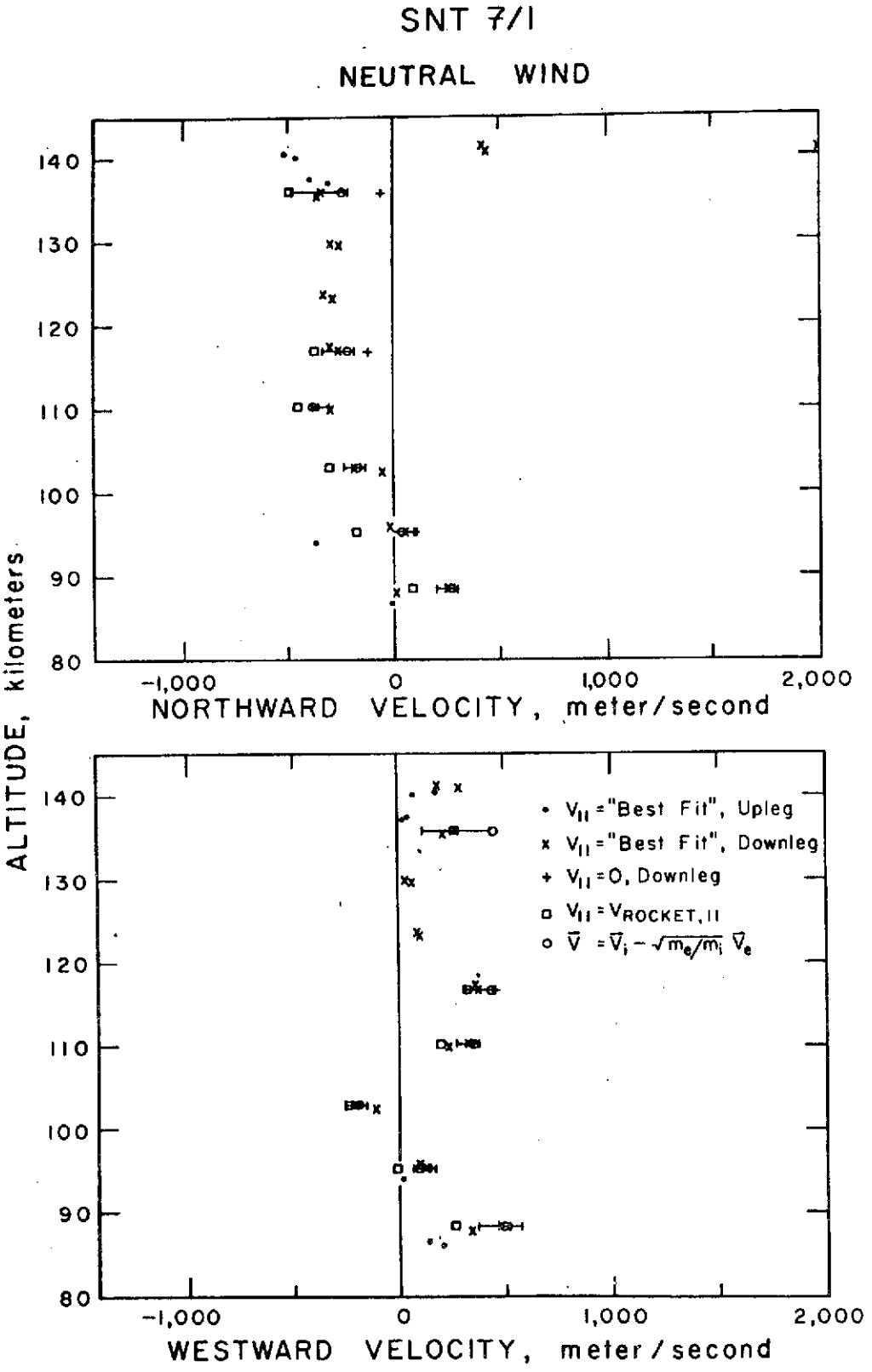
SNT 7/1
NEUTRAL WIND
ALTITUDE, kilometers
140
130
120
110
100
90
80
-1,000
0
1,000
2,000
NORTHWARD VELOCITY, meter/second
WESTWARD VELOCITY, meter/second
• $V_{\parallel}$ = "Best Fit", Upleg
x $V_{\parallel}$ = "Best Fit", Downleg
+ $V_{\parallel}$ = 0, Downleg
□ $V_{\parallel} = V_{ROCKET,\parallel}$
○ $\bar{V} = \bar{V}_i - \sqrt{m_e/m_i}\,\bar{V}_e$

Figure 11

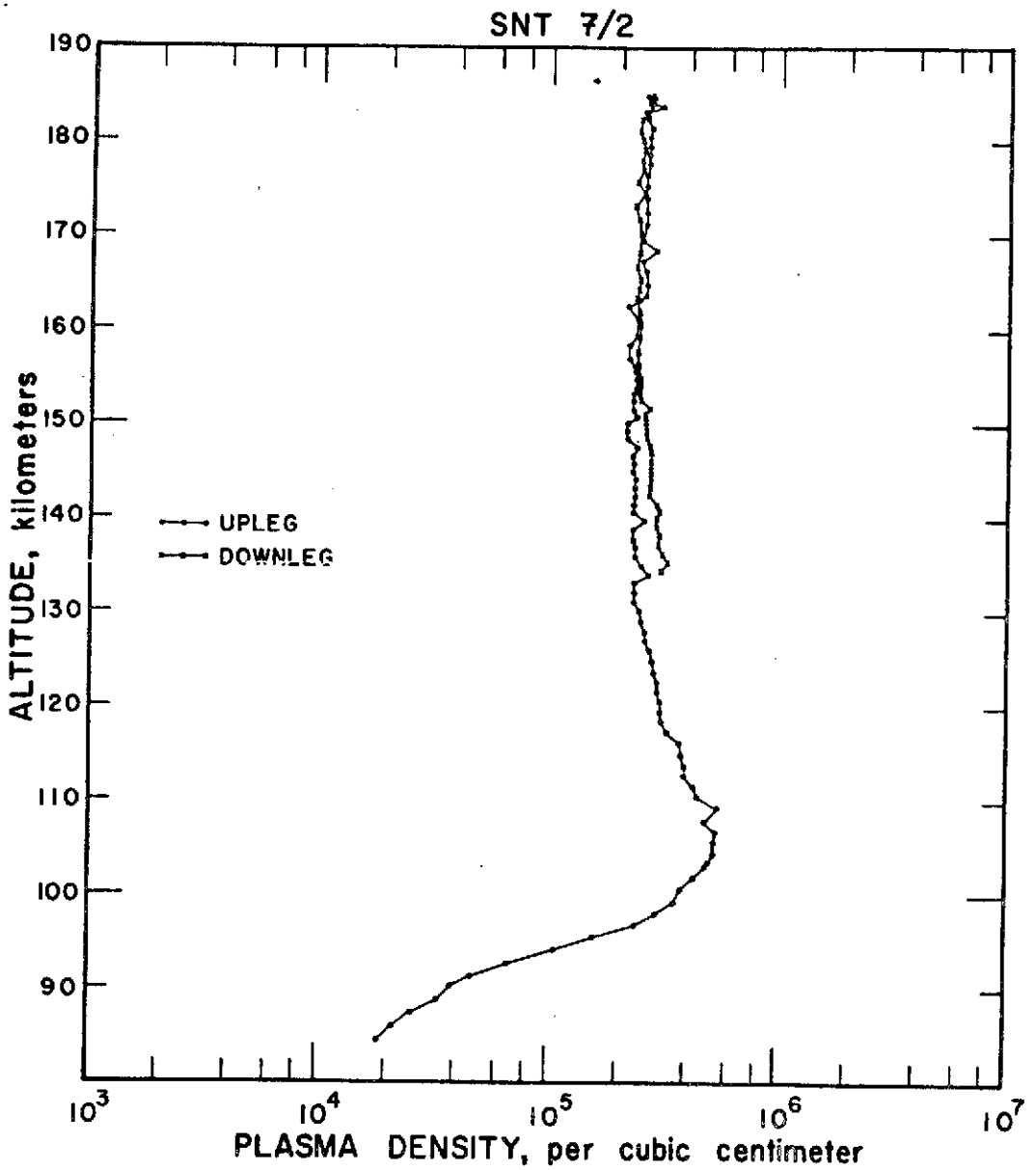
SNT 7/2
190
180
170
160
150
140
130
120
110
100
90
ALTITUDE, kilometers
UPLEG
DOWNLEG
10^3
10^4
10^5
10^6
10^7
PLASMA DENSITY, per cubic centimeter

Figure 12

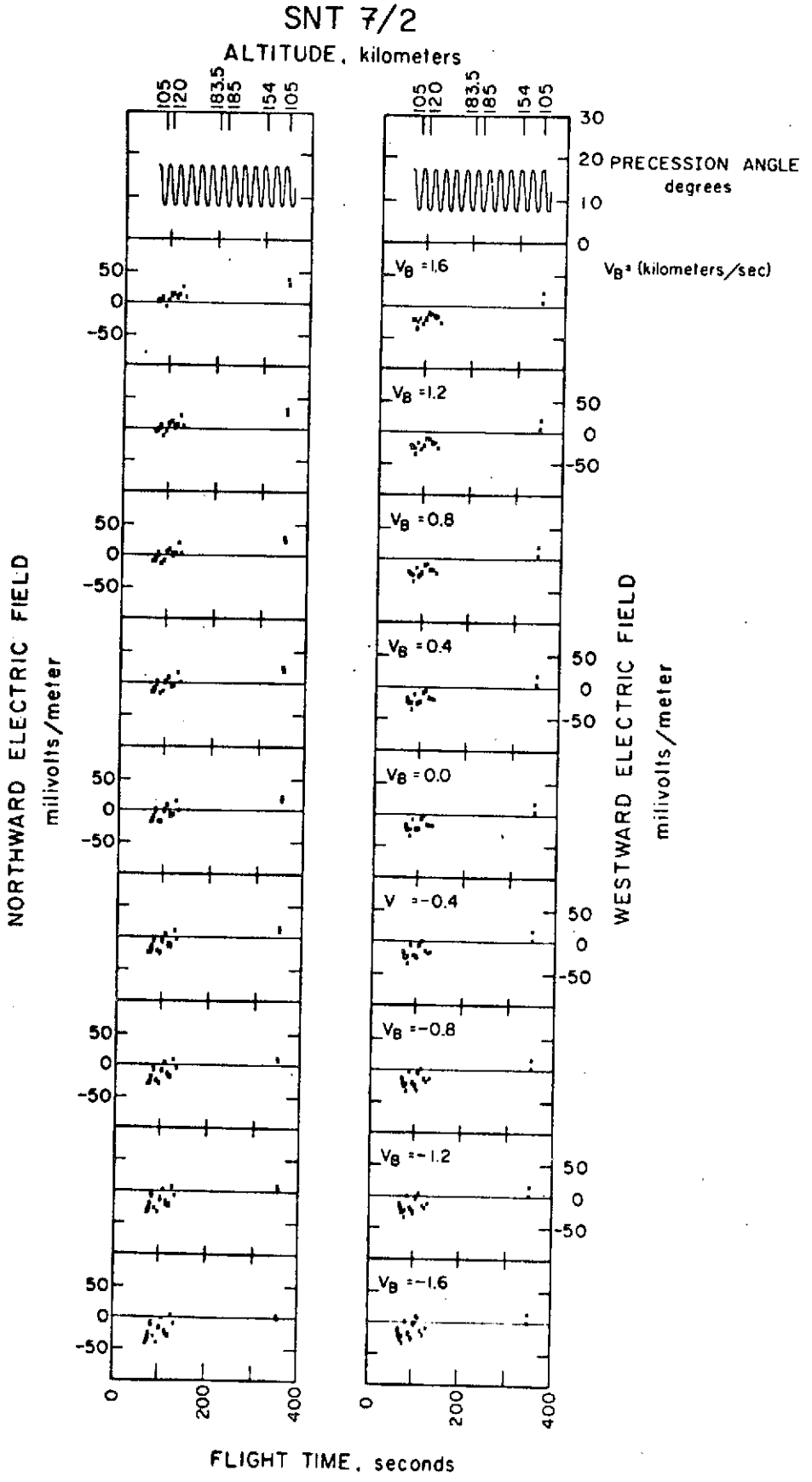
SNT 7/2
ALTITUDE, kilometers
105
120
183.5
185
154
105
PRECESSION ANGLE
degrees
30
20
10
0
V_B = (kilometers/sec)
V_B =1.6
V_B =1.2
V_B =0.8
V_B =0.4
V_B =0.0
V_B =-0.4
V_B =-0.8
V_B =-1.2
V_B =-1.6
50
0
-50
NORTHWARD ELECTRIC FIELD
milivolts/meter
WESTWARD ELECTRIC FIELD
milivolts/meter
0
200
400
FLIGHT TIME, seconds

Figure 13

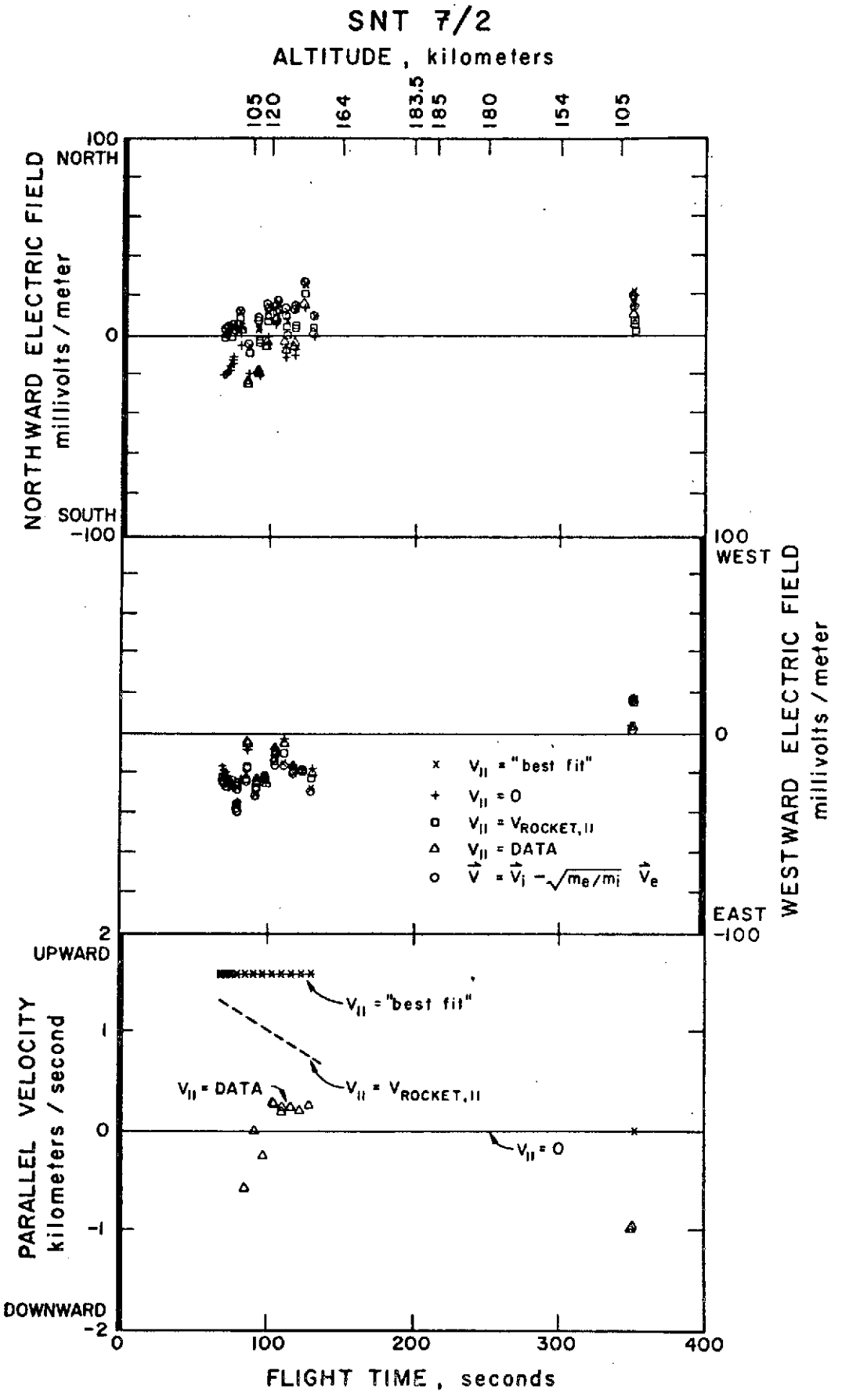
SNT 7/2
ALTITUDE , kilometers
105
120
164
183.5
185
180
154
105
NORTHWARD ELECTRIC FIELD
millivolts / meter
100
NORTH
0
SOUTH
-100
WESTWARD ELECTRIC FIELD
millivolts / meter
100
WEST
0
EAST
-100
$V_{||}$ = "best fit"
$V_{||}$ = 0
$V_{||}$ = $V_{ROCKET,||}$
$V_{||}$ = DATA
$\vec{V} = \vec{V}_i - \sqrt{m_e/m_i}\ \vec{V}_e$
PARALLEL VELOCITY
kilometers / second
2
UPWARD
1
0
-1
DOWNWARD
-2
$V_{||}$ = "best fit"
$V_{||}$ = $V_{ROCKET,||}$
$V_{||}$ = DATA
$V_{||}$ = 0
0
100
200
300
400
FLIGHT TIME , seconds

Figure 14

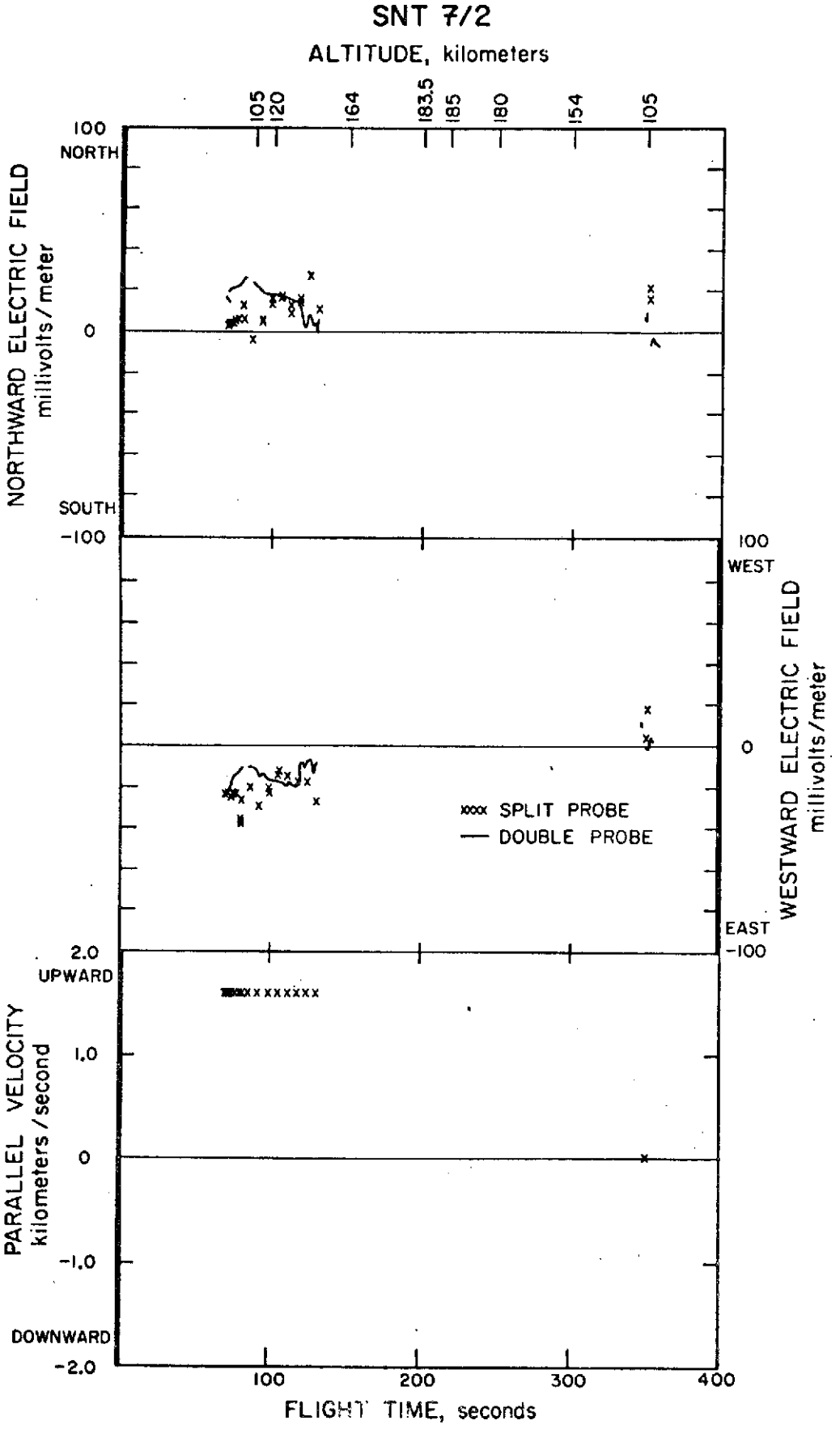
SNT 7/2
ALTITUDE, kilometers
105
120
164
183.5
185
180
154
105
100
NORTH
0
SOUTH
-100
NORTHWARD ELECTRIC FIELD
millivolts / meter
100
WEST
0
EAST
-100
WESTWARD ELECTRIC FIELD
millivolts/meter
xxxx SPLIT PROBE
— DOUBLE PROBE
2.0
UPWARD
1.0
0
-1.0
DOWNWARD
-2.0
PARALLEL VELOCITY
kilometers / second
100
200
300
400
FLIGHT TIME, seconds

Figure 15

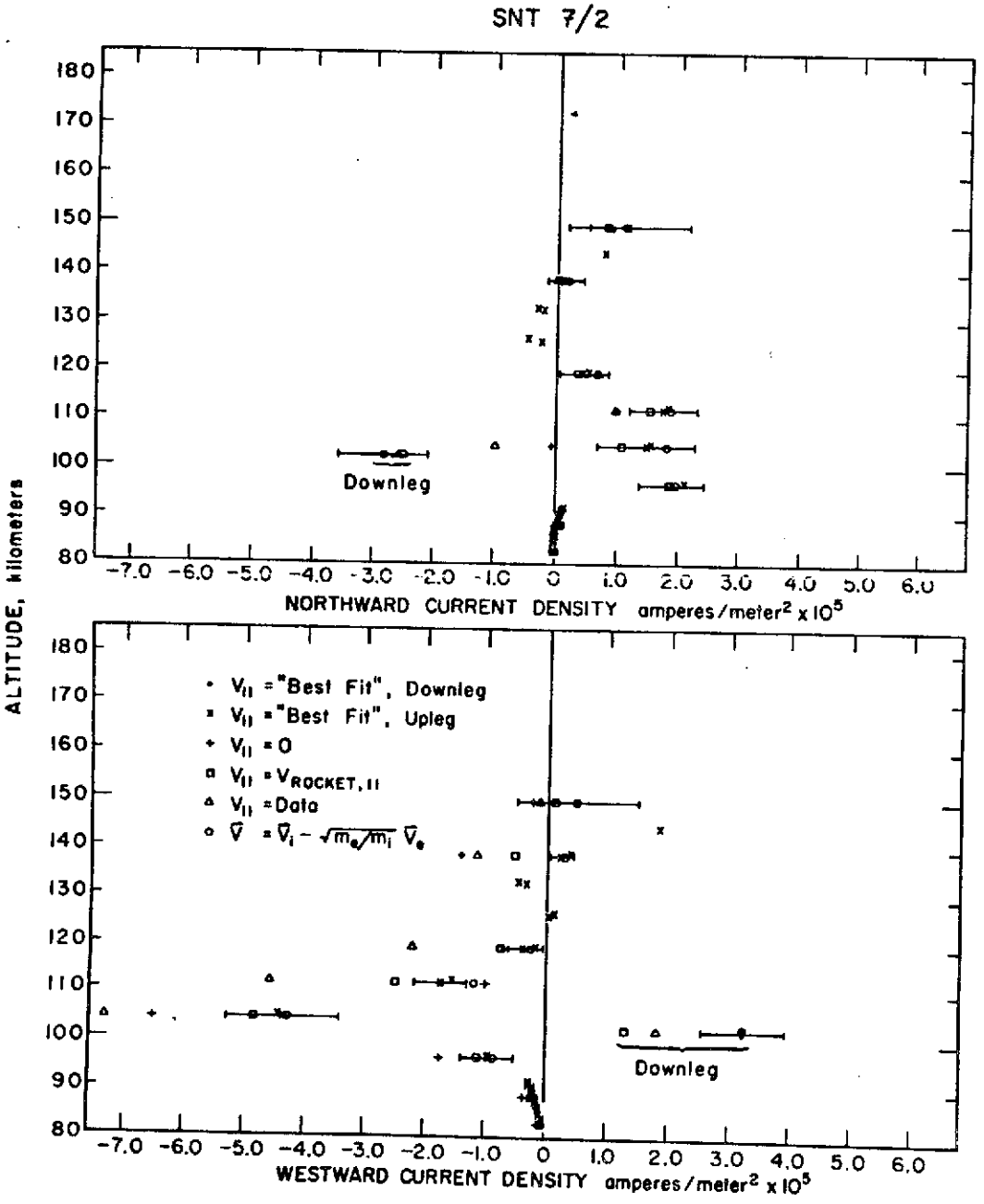
SNT 7/2
ALTITUDE, kilometers
180
170
160
150
140
130
120
110
100
90
80
Downleg
-7.0 -6.0 -5.0 -4.0 -3.0 -2.0 -1.0 0 1.0 2.0 3.0 4.0 5.0 6.0
NORTHWARD CURRENT DENSITY amperes/meter² x 10⁵
• V∥ = "Best Fit", Downleg
× V∥ = "Best Fit", Upleg
+ V∥ = 0
□ V∥ = V ROCKET, ∥
△ V∥ = Data
○ V̄ = V̄i − √(me/mi) V̄e
Downleg
WESTWARD CURRENT DENSITY amperes/meter² x 10⁵

Figure 16

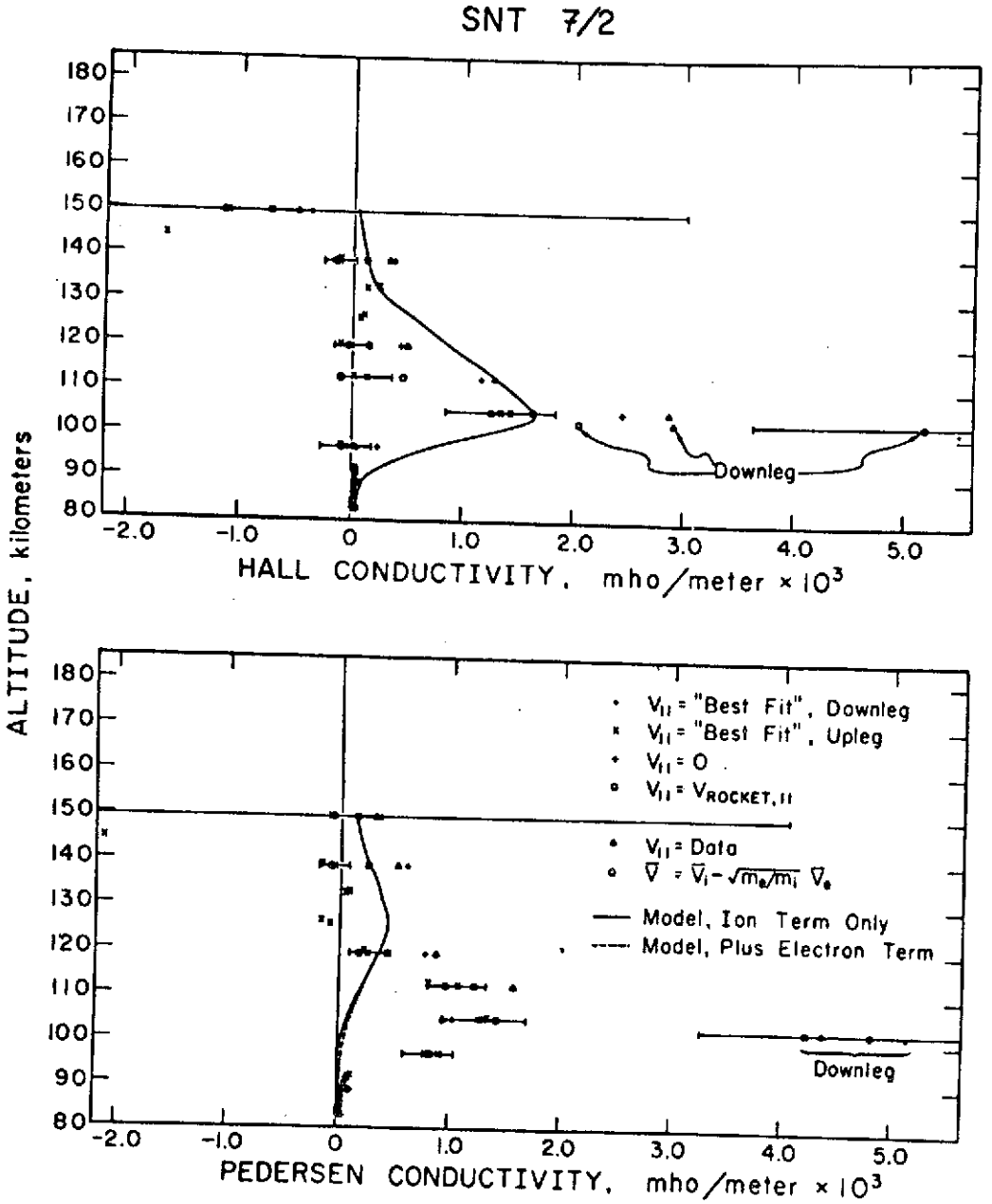
SNT 7/2
ALTITUDE, kilometers
180
170
160
150
140
130
120
110
100
90
80
-2.0
-1.0
0
1.0
2.0
3.0
4.0
5.0
Downleg
HALL CONDUCTIVITY, mho/meter × 10³
$V_{\perp\!\!\!\perp}$ = "Best Fit", Downleg
$V_{\perp\!\!\!\perp}$ = "Best Fit", Upleg
$V_{\perp\!\!\!\perp}$ = 0
$V_{\perp\!\!\!\perp}$ = $V_{ROCKET,\perp\!\!\!\perp}$
$V_{\perp\!\!\!\perp}$ = Data
$\bar{\nabla} = \bar{V}_i - \sqrt{m_e/m_i}\,\bar{V}_e$
Model, Ion Term Only
Model, Plus Electron Term
Downleg
PEDERSEN CONDUCTIVITY, mho/meter × 10³

Figure 17

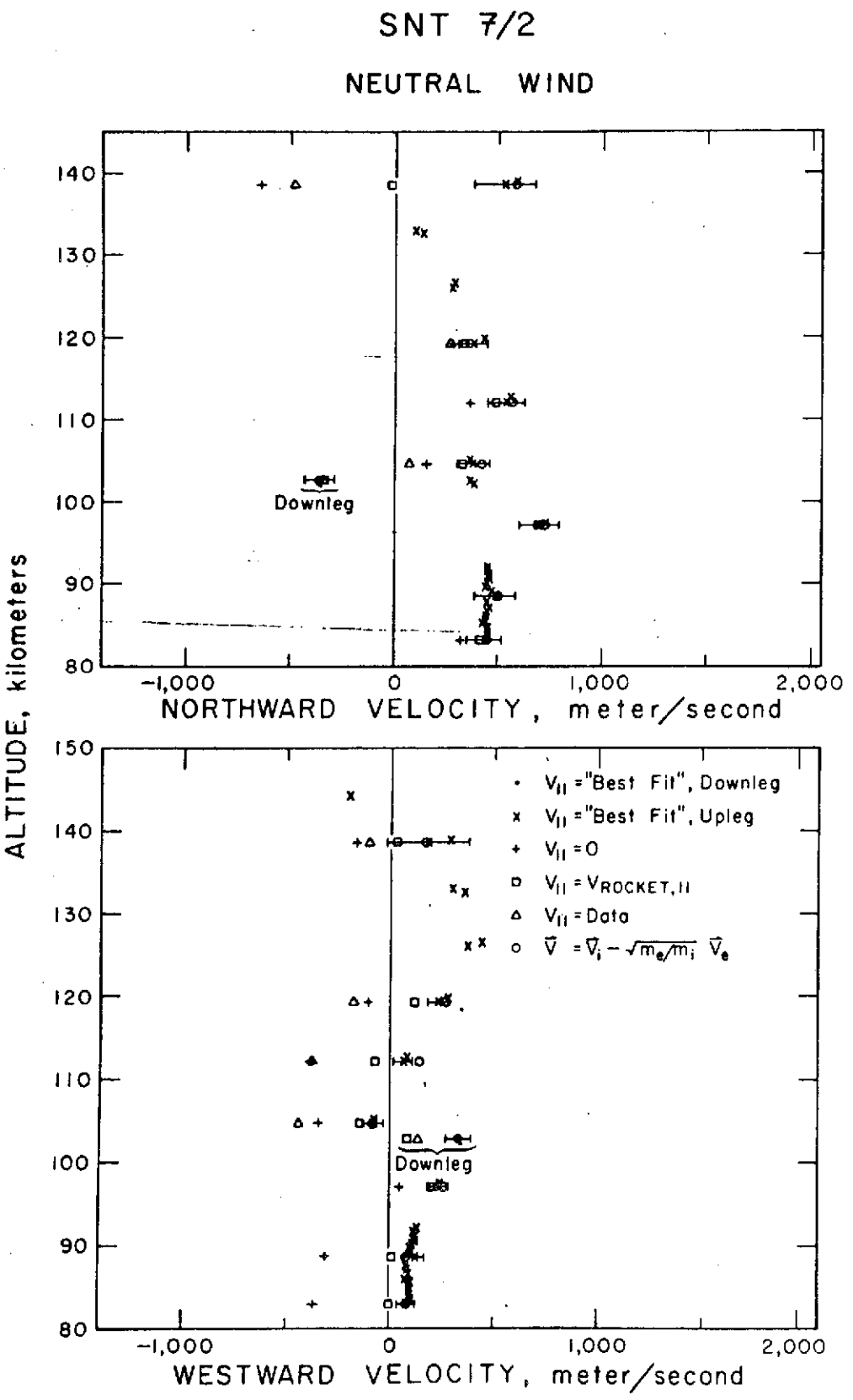
SNT 7/2
NEUTRAL WIND
ALTITUDE, kilometers
140
130
120
110
100
90
80
Downleg
-1,000
0
1,000
2,000
NORTHWARD VELOCITY, meter/second
150
140
130
120
110
100
90
80
Downleg
$V_{\parallel}$ = "Best Fit", Downleg
$V_{\parallel}$ = "Best Fit", Upleg
$V_{\parallel} = 0$
$V_{\parallel} = V_{ROCKET,\parallel}$
$V_{\parallel}$ = Data
$\vec{V} = \vec{V}_i - \sqrt{m_e/m_i}\ \vec{V}_e$
-1,000
0
1,000
2,000
WESTWARD VELOCITY, meter/second

Figure 18

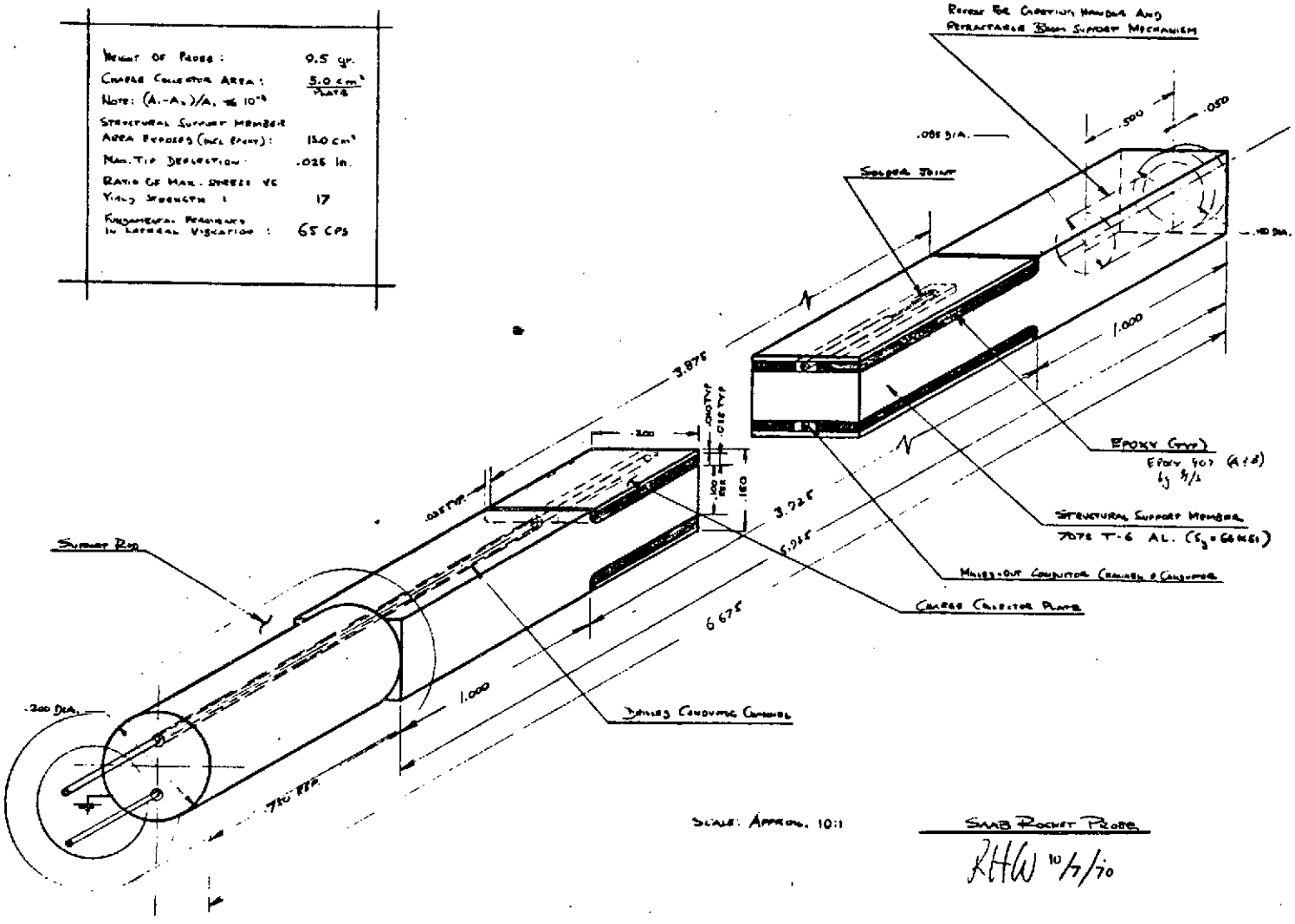
Weight of Probe : 9.5 gr.
Charge Collector Area : 5.0 cm² Plate
Note: (A.-A₀)/A₀ ≈ 10⁻⁵
Structural Support Member Area Exposed (incl Epoxy) : 13.0 cm²
Max. Tip Deflection : .026 in.
Ratio of Max. Stress vs Yield Strength : 17
Fundamental Frequency in Lateral Vibration : 65 CPS
Retract for Ejection Handle and Retractable Beam Support Mechanism
.005 S/A.
.500
.050
Solder Joint
.100 Dia.
1.000
3.875
.200
.100
.150
3.225
6.925
6.675
Epoxy (typ.)
Epoxy 907 (A+B) by Hysol
Structural Support Member 7075 T-6 Al. (Sy = 68 KSI)
Molded-Out Conductor Channels & Conductors
Charge Collector Plate
Sensor Rod
.200 Dia.
.750 Dia.
Sensor Conductor Channel
Scale: Approx. 10:1
SNAB Rocket Probe
RHW 10/7/70

Figure 19

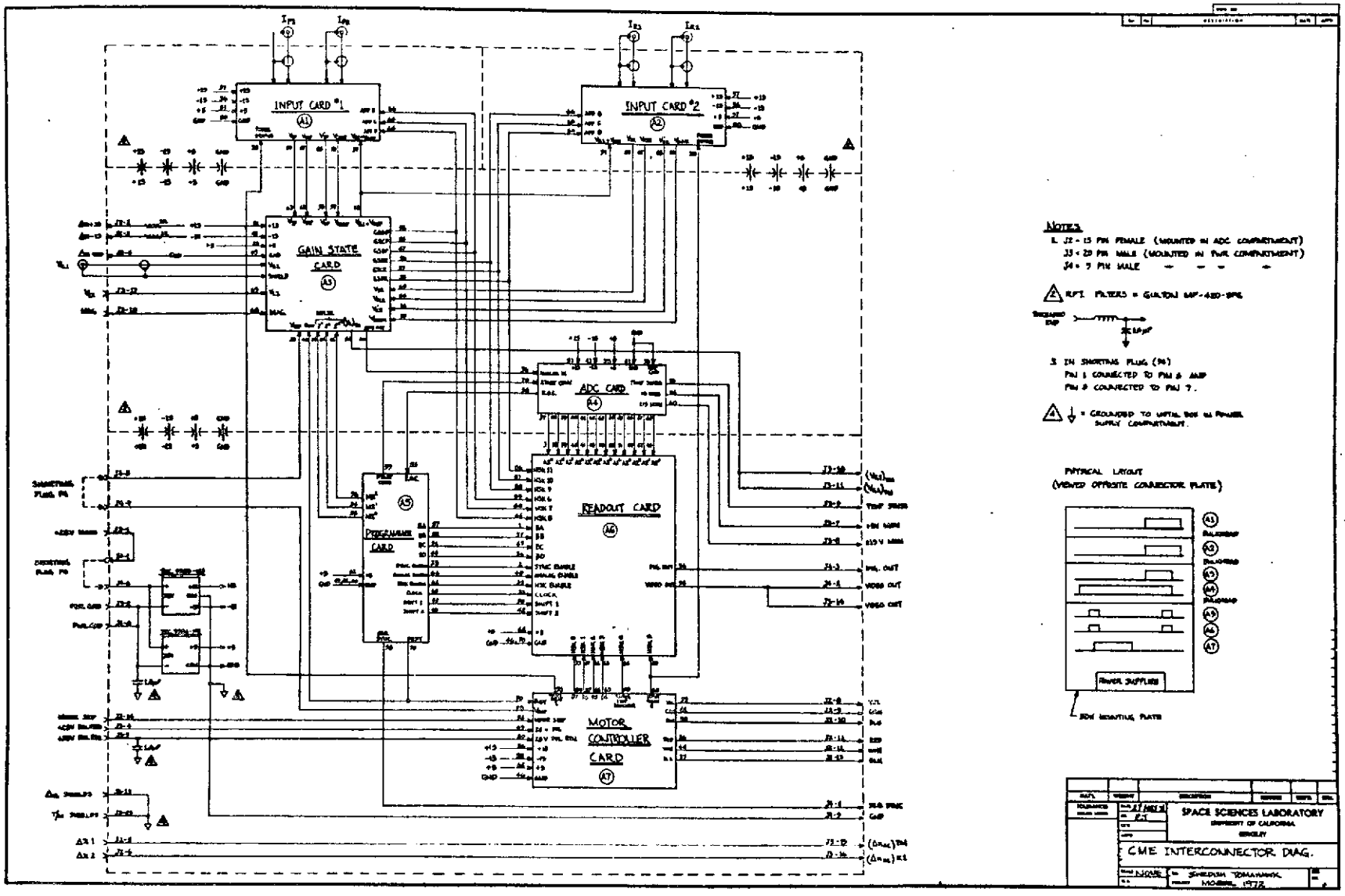
INPUT CARD #1
INPUT CARD #2
GAIN STATE CARD
ADC CARD
READOUT CARD
PROGRAMMER CARD
MOTOR CONTROLLER CARD
NOTES
SPACE SCIENCES LABORATORY
CME INTERCONNECTOR DIAG.

Figure 20

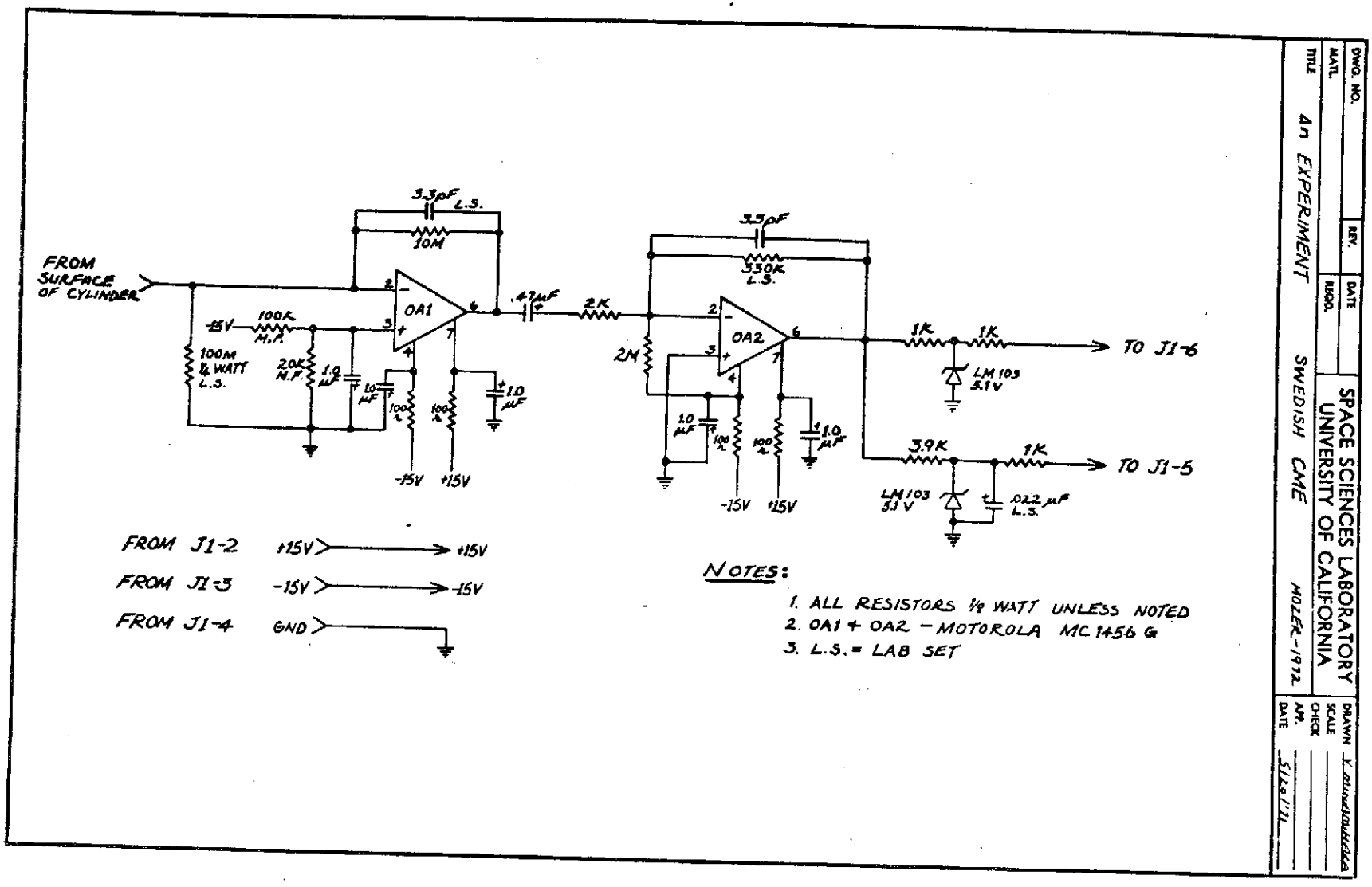
FROM SURFACE OF CYLINDER
3.3pF L.S.
10M
OA1
.47μF
2K
3.3pF
330K L.S.
OA2
2M
1K
1K
TO J1-6
LM 103 5.1V
3.9K
1K
TO J1-5
LM 103 5.1 V
.022 μF L.S.
100K M.F.
100M ½ WATT L.S.
2.0K N.F.
1.0 μF
10 μF
100 Ω
1.0 μF
-15V
+15V
FROM J1-2 +15V +15V
FROM J1-3 -15V -15V
FROM J1-4 GND
NOTES:
1. ALL RESISTORS ⅛ WATT UNLESS NOTED
2. OA1 + OA2 – MOTOROLA MC 1456 G
3. L.S. = LAB SET
TITLE 4π EXPERIMENT SWEDISH CME MOLER-1972
SPACE SCIENCES LABORATORY UNIVERSITY OF CALIFORNIA
DWG. NO.
MATL.
REV.
DESIG.
DATE
DRAWN
SCALE
CHECK
APP.
DATE

Figure 21

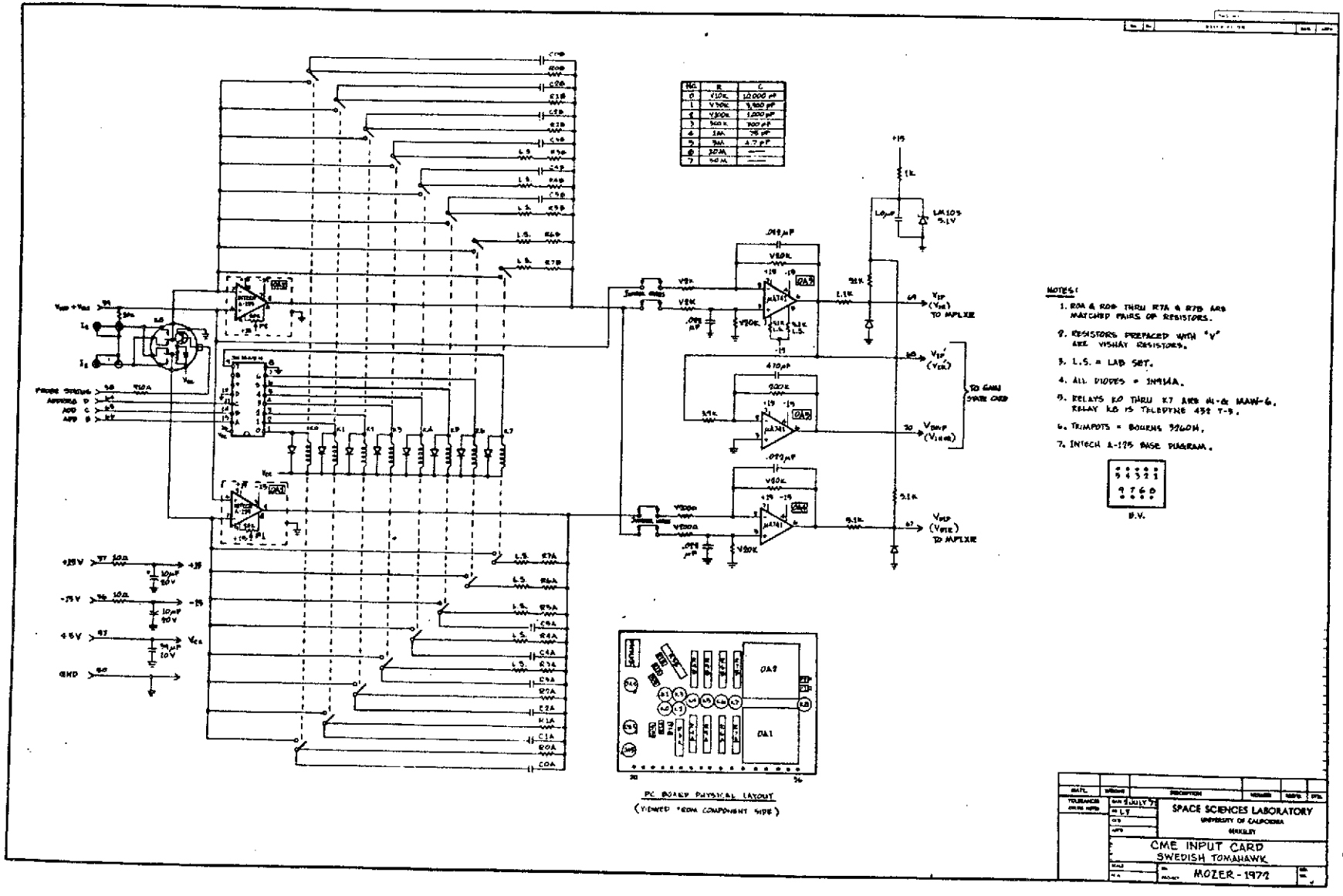
NOTES:
1. R0A & R0B THRU R7A & R7B ARE MATCHED PAIRS OF RESISTORS.
2. RESISTORS PREFACED WITH "V" ARE VISHAY RESISTORS.
3. L.S. = LAB SET.
4. ALL DIODES = IN914A.
5. RELAYS K0 THRU K7 ARE MI-4x MAW-6. RELAY K8 IS TELEDYNE 432 T-9.
6. TRIMPOTS = BOURNS 3260H.
7. INTECH A-175 BASE DIAGRAM.
PC BOARD PHYSICAL LAYOUT
(VIEWED FROM COMPONENT SIDE)
SPACE SCIENCES LABORATORY
UNIVERSITY OF CALIFORNIA
BERKELEY
CME INPUT CARD
SWEDISH TOMAHAWK
MOZER - 1972

Figure 22

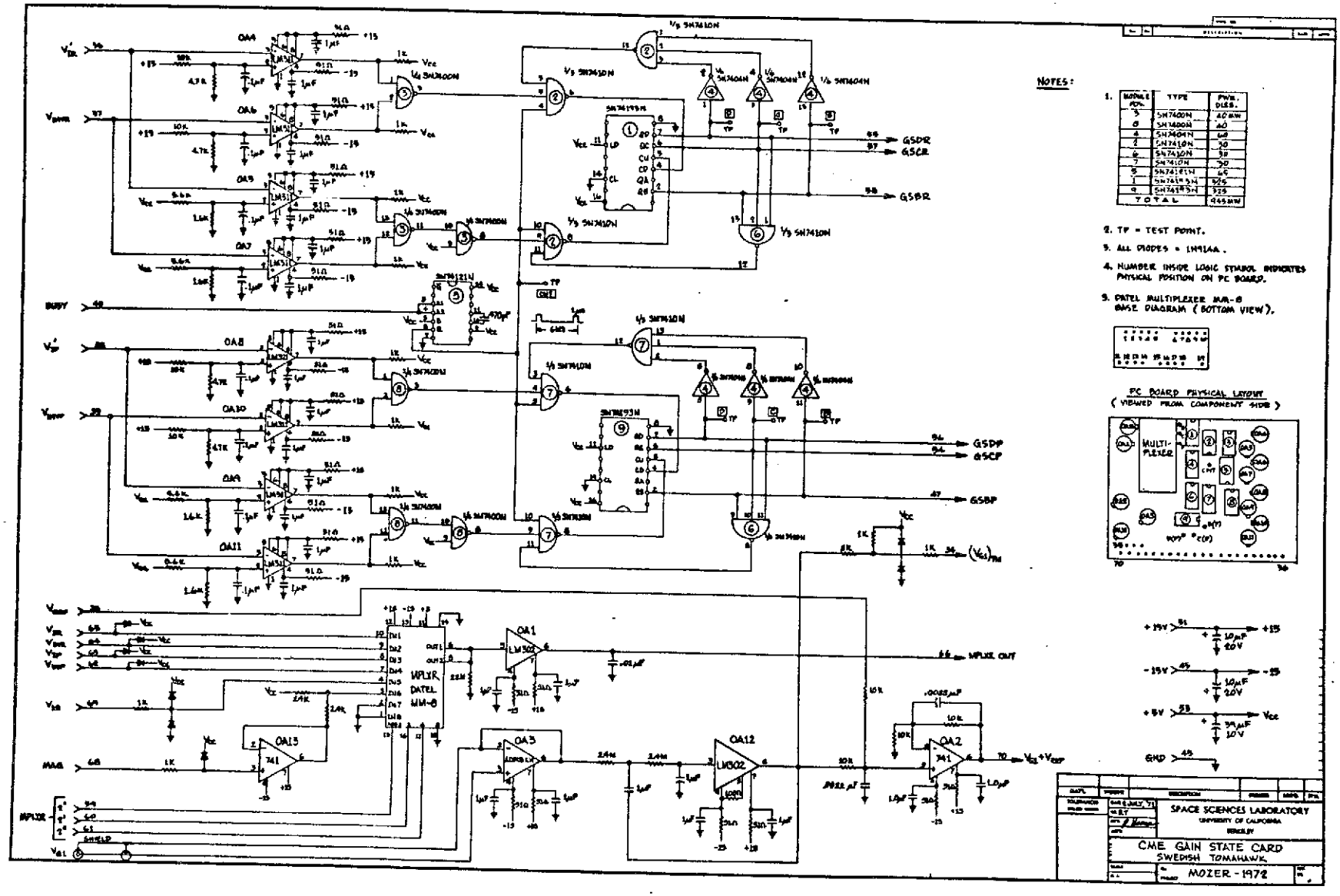
NOTES:
1.
MODULE REF. | TYPE | PWR. DISS.
5 | SN7400N | 40 MW
6 | SN7400N | 40
4 | SN7404N | 68
2 | SN7410N | 30
6 | SN7430N | 30
7 | SN7410N | 30
5 | SN7415N | 45
1 | SN7419N SN | 525
9 | SN7419N SN | 525
TOTAL | | 945 MW
2. TP = TEST POINT.
3. ALL DIODES = 1N914A.
4. NUMBER INSIDE LOGIC SYMBOL INDICATES PHYSICAL POSITION ON PC BOARD.
5. PATEL MULTIPLEXER MM-8 BASE DIAGRAM (BOTTOM VIEW).
PC BOARD PHYSICAL LAYOUT
(VIEWED FROM COMPONENT SIDE)
MULTI-PLEXER
GSDR
GSCR
GSBR
GSDP
GSCP
GSBP
MPLXR DATEL MM-8
MPLEX OUT
+15V
-15V
+5V
GND
SPACE SCIENCES LABORATORY
UNIVERSITY OF CALIFORNIA
BERKELEY
CME GAIN STATE CARD
SWEDISH TOMAHAWK
MOZER - 1972

Figure 23

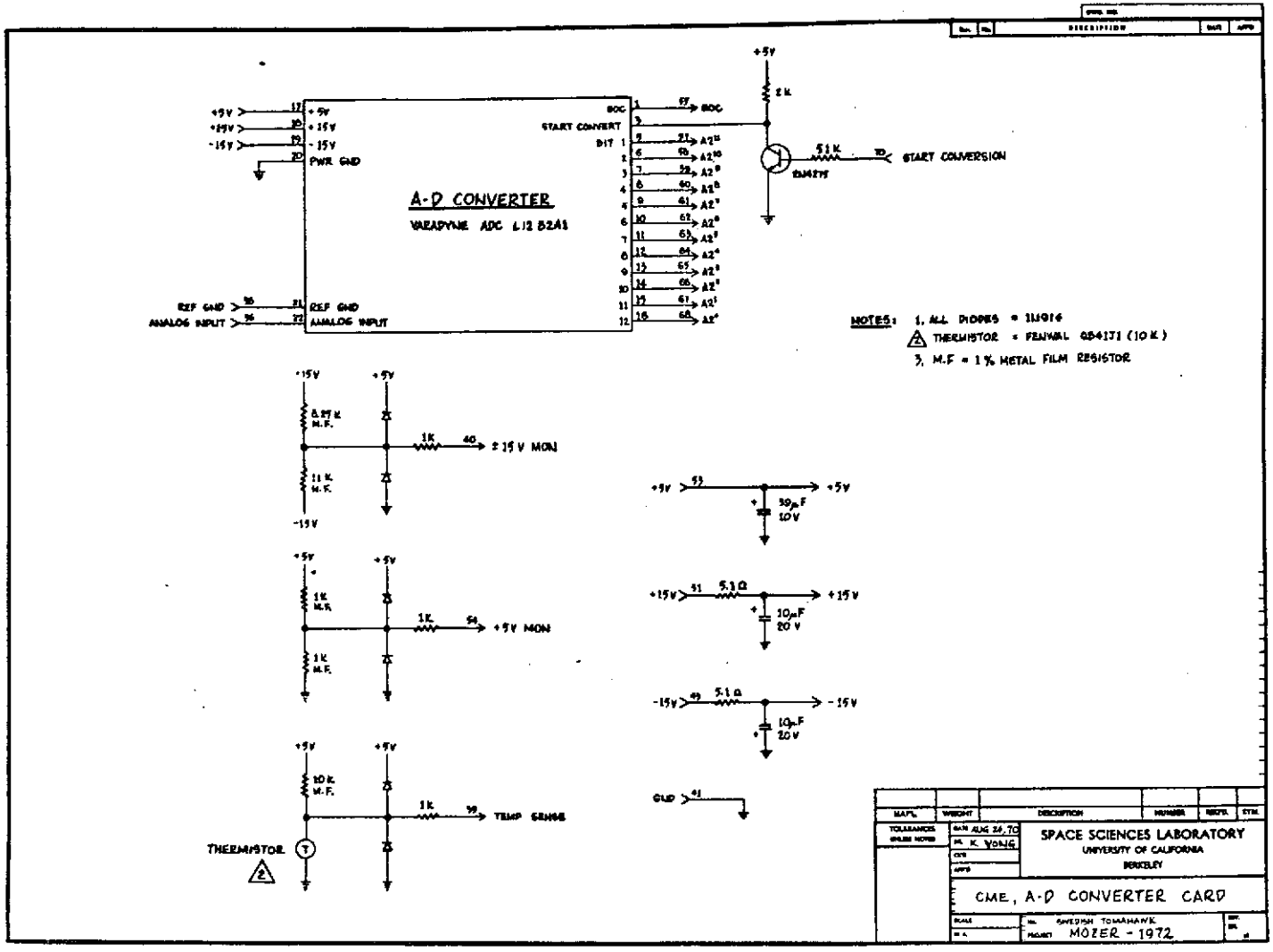
A-D CONVERTER
VARIAN ADC 612 8241
+5V
+15V
-15V
PWR GND
REF GND
ANALOG INPUT
START CONVERT
EOC
BIT 1
START CONVERSION
2N4274
5.1K
2K
NOTES: 1. ALL DIODES = 1N914
2. THERMISTOR = FENWAL GB41J1 (10K)
3. M.F. = 1% METAL FILM RESISTOR
8.87K M.F.
11K M.F.
1K
±15V MON
+5V MON
10K M.F.
TEMP SENSE
THERMISTOR
10μF 10V
10μF 20V
5.1Ω
SPACE SCIENCES LABORATORY
UNIVERSITY OF CALIFORNIA
BERKELEY
CME, A-D CONVERTER CARD
SWEDISH TOMAHAWK
MOZER - 1972

Figure 24

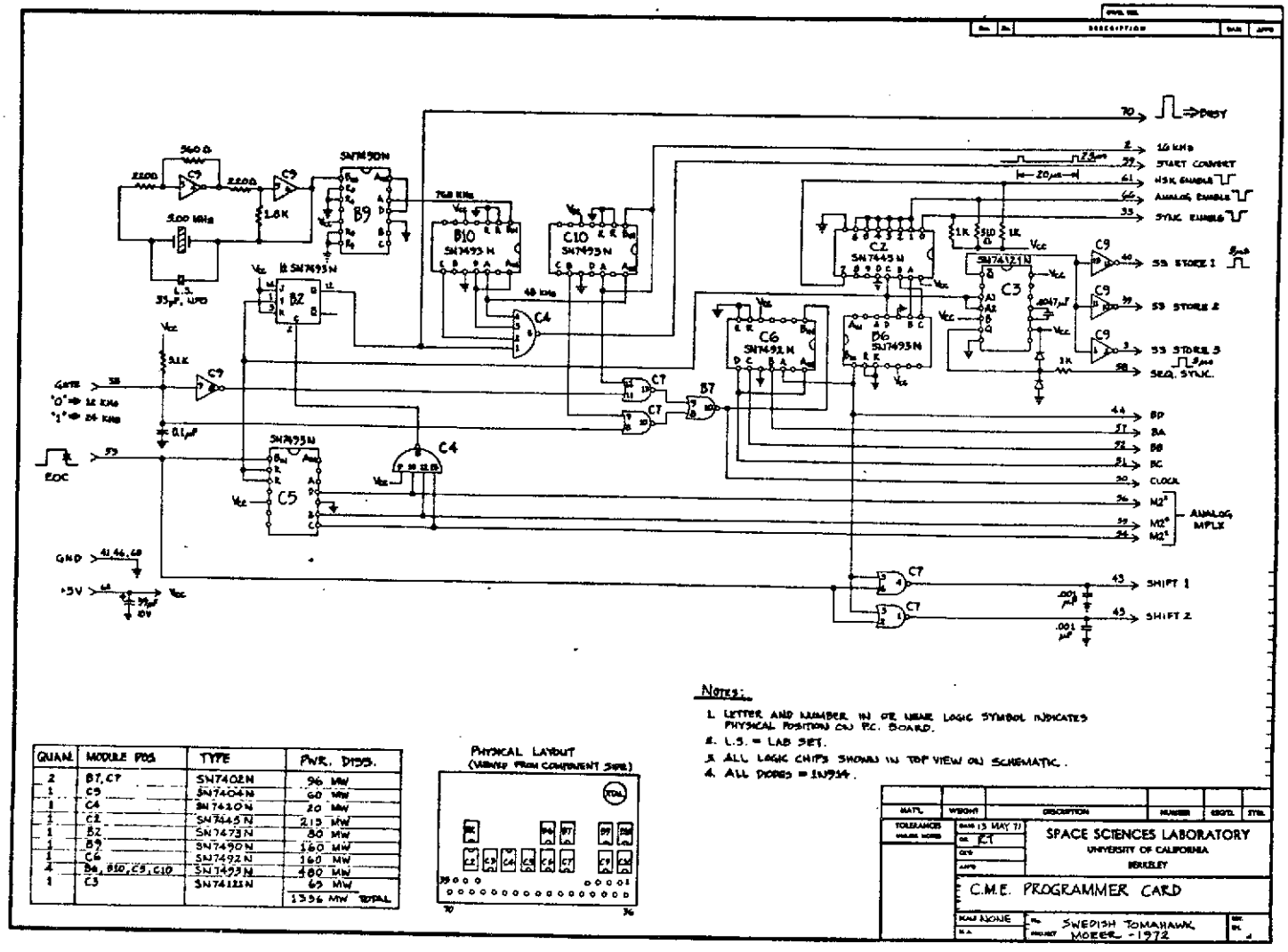

QUAN.	MODULE POS	TYPE	PWR. DISS.
2	B7, C7	SN7402N	96 MW
1	C9	SN7404N	60 MW
1	C4	SN7420N	20 MW
1	C2	SN7445N	215 MW
1	B2	SN7473N	80 MW
1	B9	SN7490N	160 MW
1	C6	SN7492N	160 MW
4	B4, B10, C9, C10	SN7493N	480 MW
1	C3	SN74121N	69 MW
			1336 MW TOTAL

Figure 25

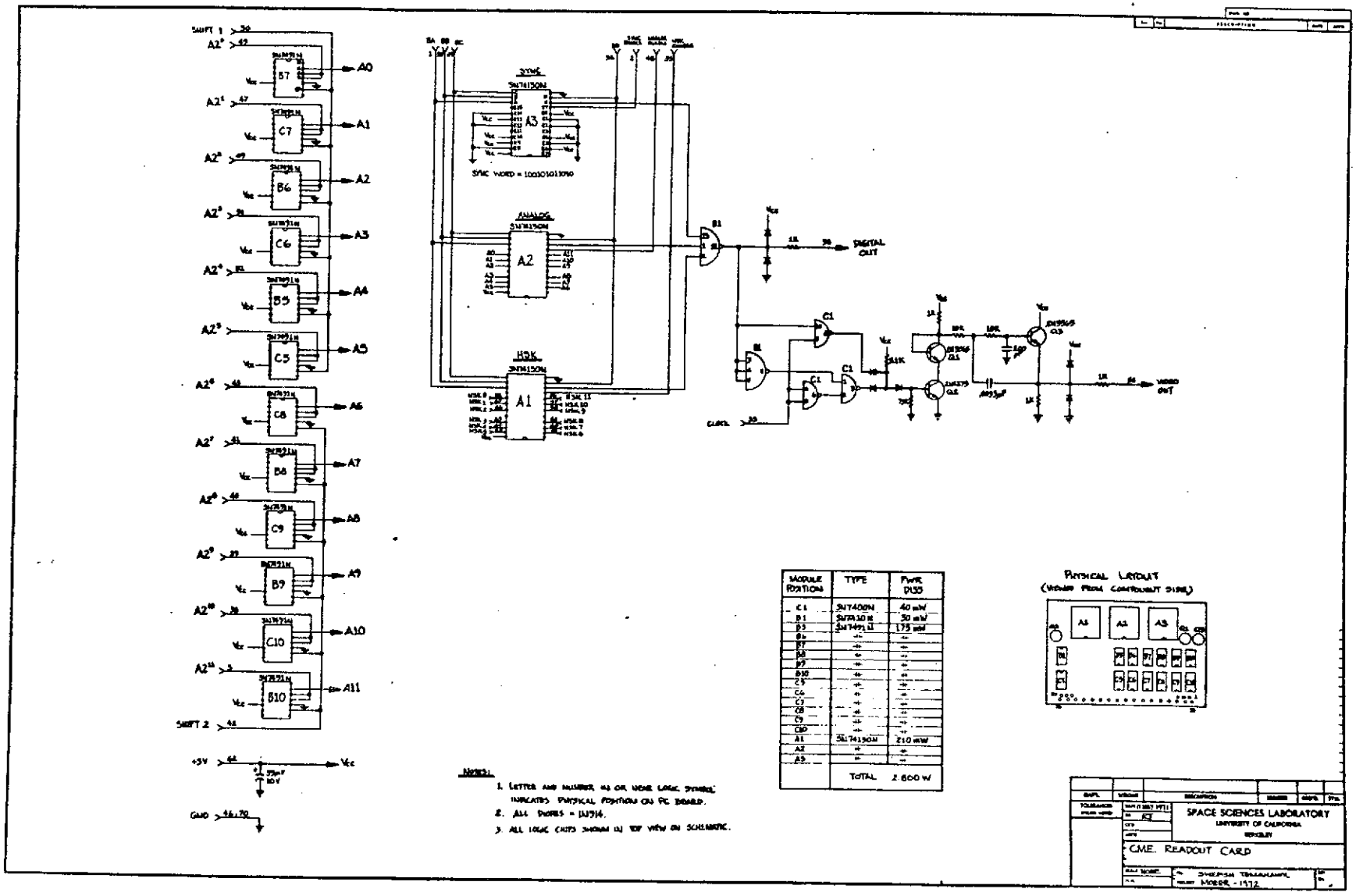
SHIFT 1
A2⁰
A2¹
A2²
A2³
A2⁴
A2⁵
A2⁶
A2⁷
A2⁸
A2⁹
A2¹⁰
A2¹¹
SHIFT 2
B7
C7
B6
C6
B5
C5
C8
B8
C9
B9
C10
B10
A0
A1
A2
A3
A4
A5
A6
A7
A8
A9
A10
A11
+5V
Vcc
GND
SYNC
A3
SYNC WORD = 1001010113090
ANALOG
A2
H9K
A1
B1
DIGITAL OUT
C1
C1
C1
CLOCK
VIDEO OUT
NOTES:
1. LETTER AND NUMBER (4) OR MORE LOGIC SYMBOL INDICATES PHYSICAL POSITION ON PC BOARD.
2. ALL DIODES = IN914.
3. ALL LOGIC CHIPS SHOWN IN TOP VIEW ON SCHEMATIC.
MODULE POSITION
TYPE
PWR DISS
C1
SN7400N
40 mW
B1
SN7810 N
50 mW
B3
SN7493 N
175 mW
A1
SN74150N
210 mW
TOTAL 2.600 W
PHYSICAL LAYOUT
(VIEWED FROM COMPONENT SIDE)
A3
A2
A1
SPACE SCIENCES LABORATORY
UNIVERSITY OF CALIFORNIA
BERKELEY
CME. READOUT CARD
MODEL - 1972

Figure 26

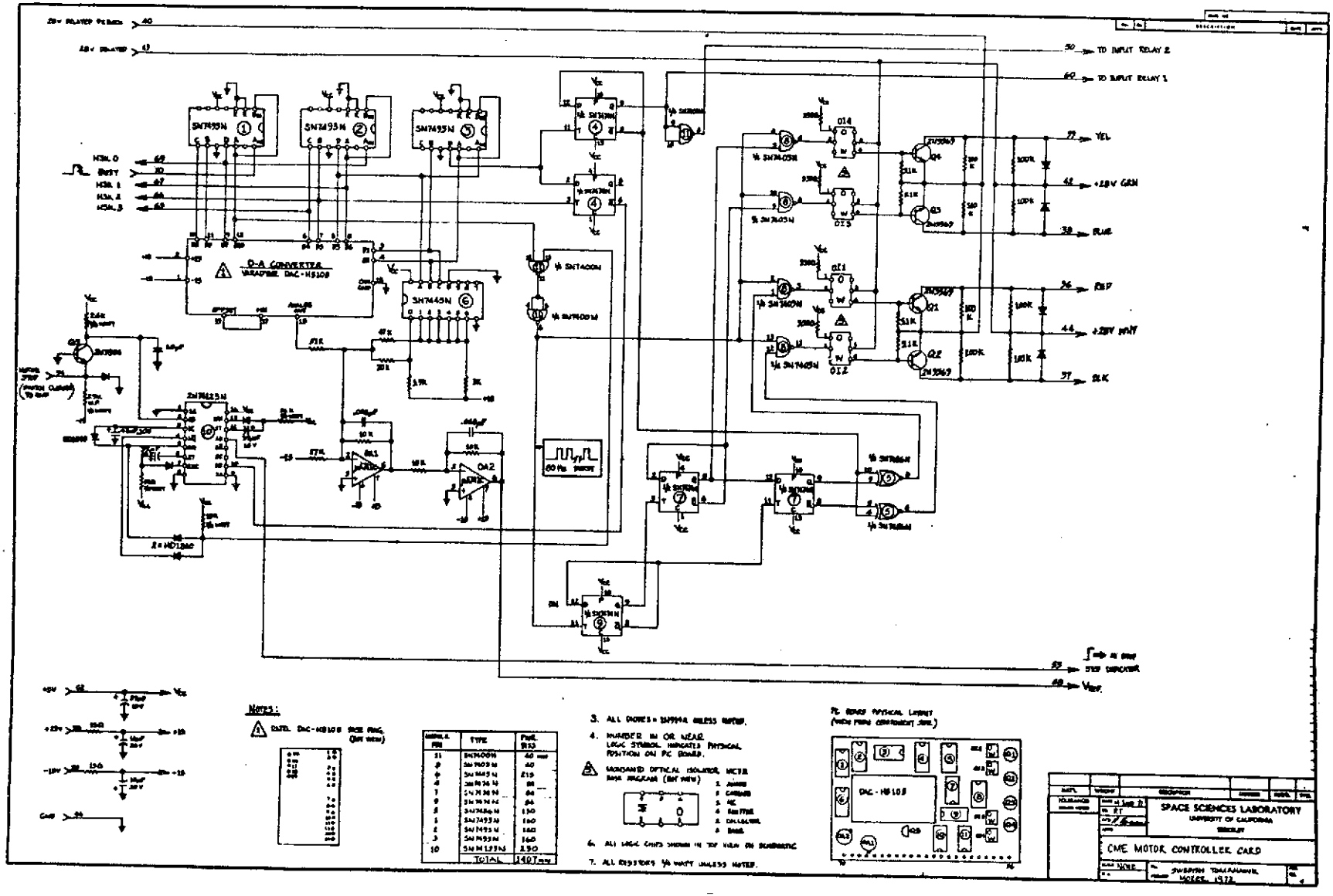
TO INPUT RELAY 2
TO INPUT RELAY 1
YEL
+18V GRN
BLUE
RED
+28V UNIT
BLK
D-A CONVERTER
VARIAN DAC-H5108
SPACE SCIENCES LABORATORY
UNIVERSITY OF CALIFORNIA
CME MOTOR CONTROLLER CARD

Figure 27

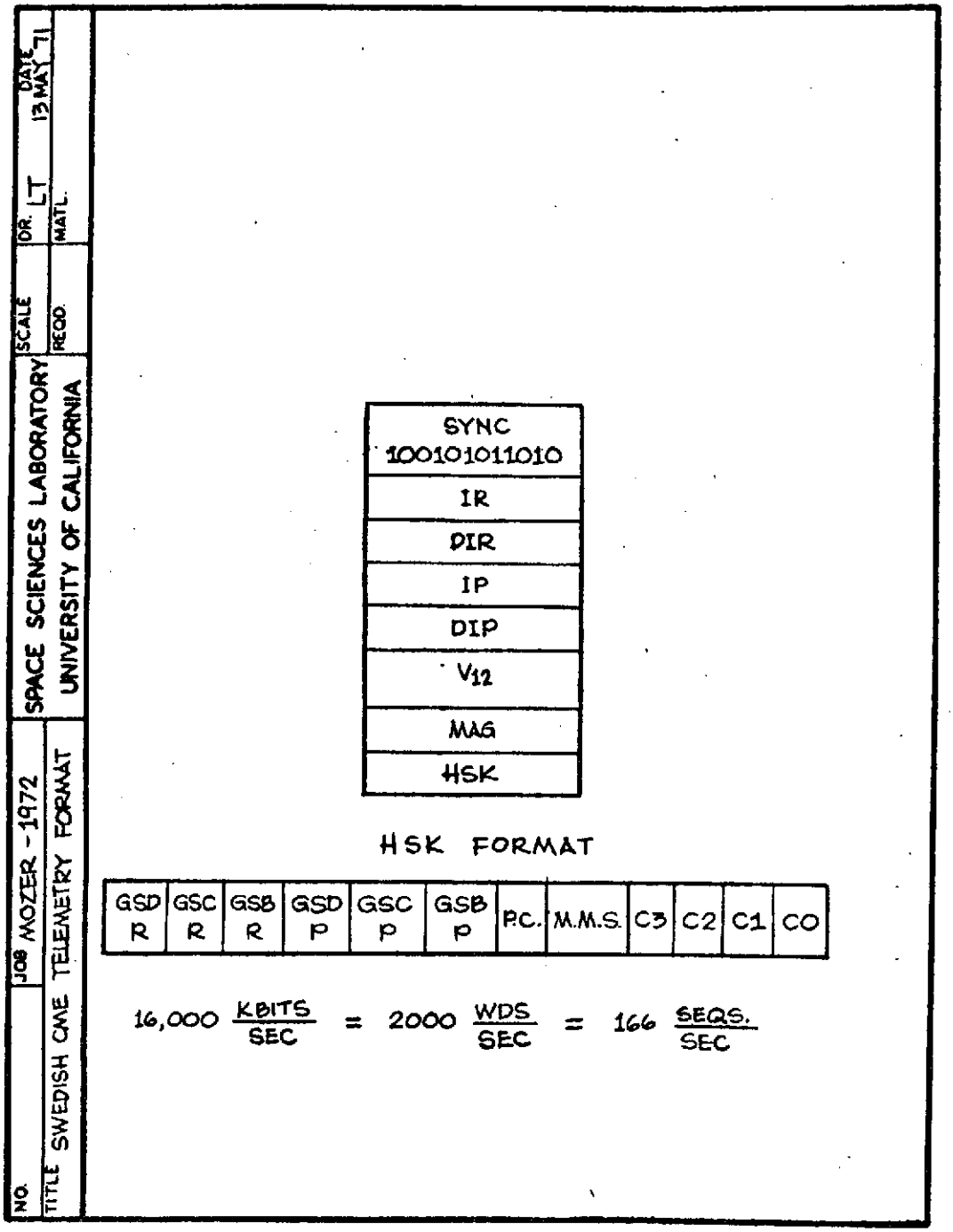
NO.
TITLE SWEDISH CME TELEMETRY FORMAT
JOB MOZER - 1972
SPACE SCIENCES LABORATORY
UNIVERSITY OF CALIFORNIA
SCALE
REQD.
DR. LT
MATL.
DATE 13 MAY 71
SYNC 100101011010
IR
DIR
IP
DIP
V12
MAG
HSK
HSK FORMAT
GSD R
GSC R
GSB R
GSD P
GSC P
GSB P
P.C.
M.M.S.
C3
C2
C1
C0
16,000 KBITS/SEC = 2000 WDS/SEC = 166 SEQS./SEC

Figure 28

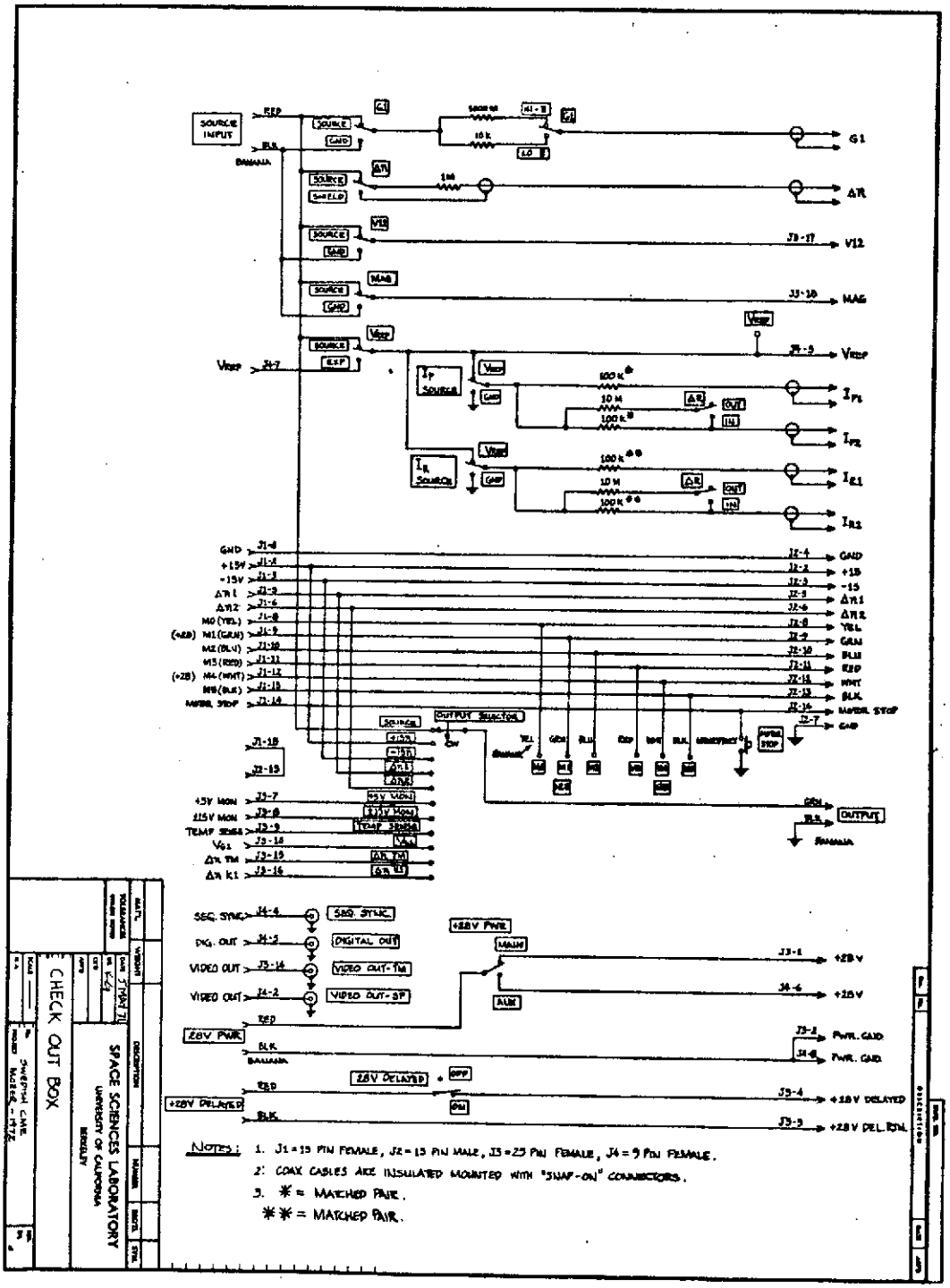
SOURCE INPUT
CHECK OUT BOX
SPACE SCIENCES LABORATORY
UNIVERSITY OF CALIFORNIA
BERKELEY
SEQ. SYNC
DIG. OUT
VIDEO OUT
+28V PWR
+28V DELAYED
NOTES:
1. J1 = 15 PIN FEMALE, J2 = 15 PIN MALE, J3 = 25 PIN FEMALE, J4 = 9 PIN FEMALE.
2. COAX CABLES ARE INSULATED MOUNTED WITH "SNAP-ON" CONNECTORS.
3. * = MATCHED PAIR.
** = MATCHED PAIR.

Figure 29

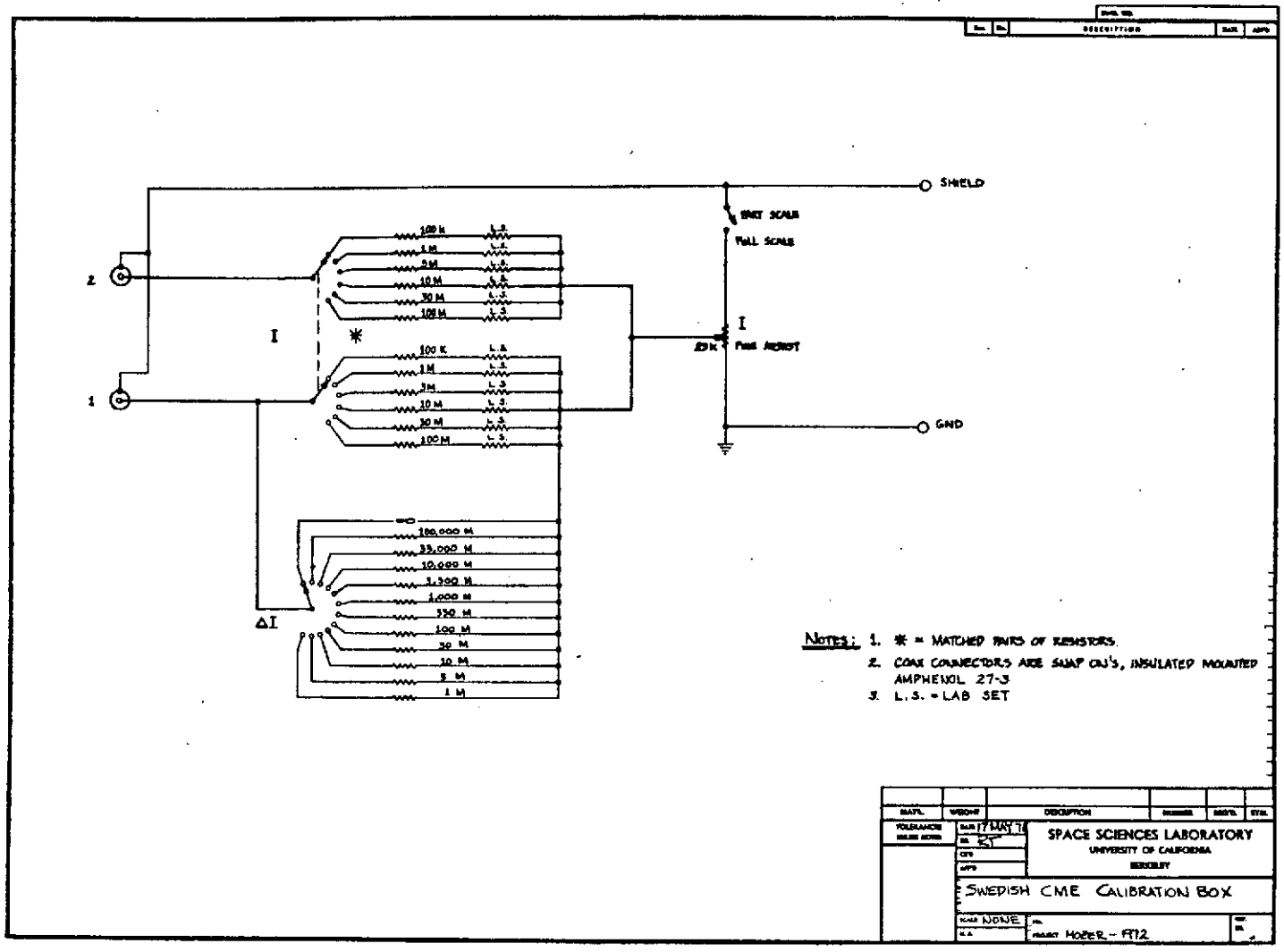
SHIELD
FULL SCALE
I
GND
2
1
100 K
1 M
3 M
10 M
30 M
100 M
ΔI
100,000 M
33,000 M
10,000 M
3,300 M
1,000 M
330 M
100 M
30 M
10 M
3 M
1 M
NOTES: 1. * = MATCHED PAIRS OF RESISTORS.
2. COAX CONNECTORS ARE SNAP ON'S, INSULATED MOUNTED AMPHENOL 27-3
3. L.S. = LAB SET
SPACE SCIENCES LABORATORY
UNIVERSITY OF CALIFORNIA
BERKELEY
SWEDISH CME CALIBRATION BOX
NONE
HOZER - FT12

Figure 30